THE ELECTROMIGRATION- AND TEMPERATURE-INDUCED STRUCTURAL BEHAVIOR OF GOLD THIN FILMS BASED UPON ALKALI ADDITIONS

By

SUSAN MATTS GOHO

A DISSERTATION PRESENTED TO THE GRADUATE SCHOOL OF
THE UNIVERSITY OF FLORIDA
IN PARTIAL FULFILLMENT OF THE REQUIREMENTS FOR THE
DEGREE OF DOCTOR OF PHILOSOPHY

UNIVERSITY OF FLORIDA

1983

ACKNOWLEDGEMENTS

The author is ultimately indebted to W. Michael Goho for his interest and encouragement during the study and research leading to this dissertation. More specifically, his unending patience, genuine intellectual varsatility and overwhelming desire to communicate the excitement of discovering the intricacies of the physical sciences afforded the author an exceptionally creative atmosphere in which to work.

Dr. R. E. Hummel is thanked for his constant support and his advice during research in a most fascinating area of materials science. Our discussions allowed for the maintenance of a stimulating laboratory environment and facilitated the author's overall development as a researcher.

The author would be remiss not to acknowledge Dr. P. H. Holloway, whose unwavering commitment to research and to those who work with him often astonishes even those who know him well.

Many thanks to all the members of the dissertation committee for their time and efforts.

Finally, the author gratefully notes the financial assistance of the United States Army.

TABLE OF CONTENTS

Page

ACKNOWLEDGEMENTS....................ii

LIST OF TABLES....................v

LIST OF FIGURES....................vi

ABSTRACT....................viii

CHAPTER 1. INTRODUCTION....................1

CHAPTER 2. THEORETICAL CONSIDERATIONS....................4
- 2.1 Introduction....................4
- 2.2 Description of the General Electromigration Process..4
- 2.3 Electromigration in Thin Films....................10
  - 2.3.1 Characteristics Specific to Thin Films.......10
  - 2.3.2 Brief Survey of Thin Film EM Models..........14

CHAPTER 3. SPECIMEN PREPARATION....................17

CHAPTER 4. TEMPERATURE-INDUCED SURFACE CHANGES IN GOLD THIN FILMS...22
- 4.1 Observation of Parallel Degradation Processes During Current Passage....................22
- 4.2 Annealing Behavior of Pure and Alloyed Gold Films...23
- 4.3 Annealing Behavior of Gold Films Due to Alkali Additions....................29

CHAPTER 5. ELECTROMIGRATION-INDUCED STRUCTURAL CHANGES IN GOLD THIN FILMS DUE TO ALKALI ADDITIONS....................39
- 5.1 General Electromigration Test Conditions............39
- 5.2 Scanning Electron Microscope Results and Analysis...39
- 5.3 Compositional Analysis Using Auger Electron Spectroscopy (AES)....................59
  - 5.3.1 General Description of AES....................59
  - 5.3.2 AES Experimental Results and Analysis........63

CHAPTER 6. REACTIVE NATURE OF THE ALKALI ELEMENTS....................77
- 6.1 Introduction....................77
- 6.2 High Alkali Mobility in Glassy Structures...........79
- 6.3 Free Energy of Alkali Oxide Formation...............84
- 6.4 Size Considerations....................90
- 6.5 Surface Energy Reduction....................91
- 6.6 The Effect of Adsorption on Surface Diffusion......100

TABLE OF CONTENTS (continued)

Page

CHAPTER 7. SUMMARY DISCUSSION....102
- 7.1 Review of Present Work in Relation to Other EM Studies....102
- 7.2 Additional Considerations....112

APPENDIX: INDICATION OF COMPETING MECHANISMS DURING DC STRESSING....116

REFERENCES....122

BIOGRAPHICAL SKETCH....129

LIST OF TABLES

Page

Table 1. Composition of Borosilicate Glasses Used as Substrates for Alloyed Gold Films....................................18

Table 2. Physical Characteristics and Test Conditions for Gold Films Used in SEM Study of Electromigration................43

Table 3. AES Parameters for Selected Elements.......................64

Table 4. Physical Characteristics and Test Conditions for Gold Films Used in AES Study of Electromigration................69

Table 5. Bonding Characteristics of Glass Constituents..............81

Table 6. Standard Gibbs Free Energy of Formation, ΔG^o...............86

Table 7. Experimental Values for Selected Surface Energies..........93

Table 8. Calculated Values of Selected Solid-Vapor Surface Energies..98

Table 9. Experimental Electromigration and Associated Diffusion Parameters Pertinent to Gold.............................103

LIST OF FIGURES

Page

Figure 1. Annealing Behavior of Pure Gold Thin Films (Quartz Substrates)....................................25

Figure 2. Annealing Behavior of Gold Thin Films (Na-Glass Substrates)..26

Figure 3. Annealing Behavior of Gold Thin Films (135 Å Intermediate Indium Layers on Quartz Substrates)...............27

Figure 4. Annealing Behavior of Gold Thin Films (Lithium Borosilicate Substrates).................................32

Figure 5. Annealing Behavior of Gold Thin Films (Sodium Borosilicate Substrates).................................34

Figure 6. Annealing Behavior of Gold Thin Films (Potassium Borosilicate Substrates).................................36

Figure 7. Pure 870 Å Gold Film Surface Following Current Passage of 7.53×10^5 Amps/cm^2 for More Than 2200 Hours...........41

Figure 8. Pure 1000 Å Gold Film Surface Following Current Passage of 6.09×10^5 Amps/cm^2 for More Than 2200 Hours...........42

Figure 9. Electromigration Damage Along 800 Å Gold Thin Film Surface (Lithium Borosilicate Substrate)..................46

Figure 10. Electromigration Damage Along 800 Å Gold Thin Film Surface (Lithium Borosilicate Substrate)..................47

Figure 11. Electromigration Damage Along 810 Å Gold Thin Film Surface (Lithium Borosilicate Substrate)..................48

Figure 12. Electromigration Failure of 800 Å Gold Thin Film (Sodium Borosilicate Substrate)..........................51

Figure 13. Low Magnification (30X) Micrograph of Current-Stressed 800 Å Gold Thin Film (Sodium Borosilicate Substrate)......52

Figure 14. Electromigration Failure of 810 Å Gold Thin Film (Sodium Borosilicate Substrate)..........................53

LIST OF FIGURES (continued)

Page

Figure 15. Electromigration Damage Along 810 Å Gold Thin Film Surface (Sodium Borosilicate Substrate)..................54

Figure 16. Electromigration Damage Along 800 Å Gold Thin Film Surface (Potassium Borosilicate Substrate)...............57

Figure 17. Electromigration Failure of 800 Å Gold Thin Film (Potassium Borosilicate Substrate).......................58

Figure 18. Atomic Number Dependence of the Mean Auger Yield.........61

Figure 19. Examples of Auger Spectra from Gold Thin Film Surfaces that Contain Various Amounts of Potassium................67

Figure 20. Variation in Normalized Auger Peak Height Ratios as a Function of Position Along the Surface of an As-Deposited Gold Thin Film (Potassium Borosilicate Substrate)........70

Figure 21. Variation in Normalized Auger Peak Height Ratios as a Function of Position Along the Surface of a Current-Stressed Gold Thin Film (Potassium Borosilicate Substrate)..72

Figure 22. Variation in Normalized Auger Peak Height Ratios as a Function of Position Along the Surface of a Current-Stressed Gold Thin Film (Potassium Borosilicate Substrate)..74

Figure 23. Variation in Normalized Auger Peak Height Ratios as a Function of Position Along the Surface of a Current-Stressed Gold Thin Film (Potassium Borosilicate Substrate)..76

Figure A-1. Failure Location Variation in Pure Au Films as a Function of Maximum Temperature Location................117

Figure A-2. Electromigration Failure Location Variation in Au Films on Intermediate In Adhesion Layer as a Function of Maximum Temperature Location............................118

Abstract of Dissertation Presented to the Graduate School
of the University of Florida in Partial Fulfillment of the
Requirements for the Degree of Doctor of Philosophy

THE ELECTROMIGRATION- AND TEMPERATURE-INDUCED STRUCTURAL BEHAVIOR OF GOLD THIN FILMS BASED UPON ALKALI ADDITIONS

By

SUSAN MATTS GOHO

December 1983

Chairman: Rolf E. Hummel

Major Department: Materials Science and Engineering

The behavior of 800 Å Au thin films deposited on alkali-borosilicate substrates is examined. The alkali elements--Li, Na and K--leave the glass substrate, enter the film and migrate along the film's grain boundaries when the films are annealed at moderate temperatures (200-560^{o}C) for short times or when the films are subjected to dc current passage. As part of the thin film system, the alkali ions are affected by the processes that cause movement of the loosely bound Au atoms that line the same boundaries.

As current is passed through a gold film, migration of both solute and solvent is stimulated by the applied electric field and by the associated rise in temperature. In all film compositions studied, including pure Au, the electron wind force is shown to dominate and is characterized by the accumulation of Au and alkali ions at the anode. This result indicates that the effective charge, Z*, for Au^+ in Au, Li^+ in Au, Na^+ in Au and K^+ in Au is negative. SEM surface analysis and AES compositional analysis show that accumulation of the alkali constituent at the anode causes severe sample degradation through rapid grain boundary grooving and associated hole formation produced by alkali mixing along the film's grain boundaries and surface.

Such Au surface roughening occurs since alkali additions to Au are expected to lower the solvent surface energy and to increase Au surface diffusion. Simultaneously, the alkali elements readily form oxides/compounds along the Au surface thereby reducing the solute's chemical potential. The catalytic nature of solute chemical potential reduction and solvent surface energy reduction is noted in rapid degradation of alkali-doped Au films subjected to short isothermal heating regimes.

The degree to which alkali accumulation at the anode dominates Au depletion at the cathode during dc current passage varies as a function of film composition and experimental procedure. It is demonstrated that the character of hole formation at the anode and at the cathode is indeed distinct. The alkali impurities enhance the rate of film degradation and severely alter the character of film failure when compared to pure Au.

CHAPTER 1
INTRODUCTION

Demands for improved product reliability in the semiconductor industry have caused the re-emergence of electromigration (EM) as a major area for scientific inquiry. While the materials studied and their metallurgical forms are typical of microcircuit interconnections, the EM process itself has long been understood as the fundamental aging process in metals and semiconductors that are subjected to an electric field.

Electromigration, i.e., the transport of matter with time induced by the application of an electric field, occurs regardless of the state and composition of the material examined. Generally, this directed mass transport proceeds with time until an open is produced, which prohibits further current flow. As might be expected, this mass transport can be enhanced or suppressed by changes in the current density and temperature affecting the sample. These macroscopic variations, however, only alter the rate of transport and fail to affect the character of the EM process in the specimen. Electromigration is activated by and maintained through divergencies caused by the temperature distribution during current powering and/or the material's grain boundary structure. A reduction in these divergencies provides the only solution in altering the EM mechanism.

Since the electromigration process is more pronounced in thin films, most EM work is pursued in this area. Both theoretical and experimental difficulties persist, however, because a fundamental undertanding among thin film processing, microstructure and associated properties is not nearly as developed to date as is the case for bulk materials. In the course of this work it became apparent that the compositional and microstructural changes specific to thin films not only enhance the number of competing mechanisms that occur during dc current powering but also complicate precise determination of the primary failure mechanism. The degree to which one mechanism predominates over another varies from system to system, and varies as well as a function of the experimental parameters.

If electron wind-directed EM is the dominant failure mode, failure is consistently observed as an open at the cathode due to mass depletion for metallic electron conductors such as Au. R. E. Hummel and H. M. Breitling,[1] however, observed failure due to an open at the anode during dc stressing of Au thin films. To date, this anode failure, or "reversal"[1] in failure site, could not be reconciled with accepted theoretical and experimental observations.

In addition to electromigration, however, a variety of thermally activated processes occur during current stressing. The most pronounced processes noted in this work include atom redistribution at the film surface which causes a reduction in the chemical potential of doped films and enhanced grain boundary grooving of the film surface. An understanding of the effectiveness of these two processes in conjunction with electron wind-directed mass transport in producing film failure satisfactorily describes anode failure in Au thin films that contain certain impurities.

As a result, it is the objective of this dissertation to closely examine the effect of the Group IA elements--Li, Na and K--on the behavior of thin gold films during direct current powering. SEM surface analysis and AES examination of the compositional variation along the film that are described in this study show a strong competition among several processes. These include alkali out-diffusion, alkali-enhanced grain boundary grooving and electron wind-induced migration of both the solute and solvent. It is observed that the electron wind simultaneously sweeps both Au and alkali ions towards the anode. These migrations are competitive and in the former, failure occurs by way of an open at the cathode, while in the latter, failure occurs by way of an open at the anode. It is demonstrated that the character of hole formation at the cathode due to Au depletion and at the anode due to alkali-stimulated grain boundary grooving are indeed distinct. It is also shown that the alkali impurities enhance the film degradation rate and severely alter film failure character when compared to pure Au.

Theoretical considerations that include the reduction of the system's chemical potential through alkali oxide/compound formation, the effect of the solute in altering the various surface energies of the solvent and therefore the degree of grain boundary grooving, and the importance of the film/environment interface in accelerating solute out-diffusion are discussed.

It is hoped that this study demonstrates that a detailed examination of the general behavior of dc powered thin film systems is required in order to correctly identify the appropriate theoretical and technological implications for electromigration in these systems.

CHAPTER 2
THEORETICAL CONSIDERATIONS

2.1 Introduction

The first identification of electromigration in thin films has been attributed to I. A. Blech and H. Sello.[2] Examination of the process is well documented in bulk systems of pure[3,4,5] and alloyed[6,7,8] metals; in Al,[9,10,11] Au[12,13,14] and other[15,16] metallic thin film systems; and recently, in extrinsic semiconductors.[17] The EM process has both beneficial and detrimental effects in practical applications, ranging from purification[18] to the breakdown of microcircuit components.[19,20] In addition, an understanding of electromigration offers insight into the fundamental interactions of electrons with matter.[21,22]

2.2 Description of the General Electromigration Process

In general, for any force, F_i, acting on any ion in a metallic lattice, that ion's mobility, μ_0, can be written as

$$\mu_0 = \frac{v_i}{F_i} \tag{1}$$

where v_i is the velocity of the ionic species of interest as affected by F_i.

As current passes through a conducting solid or liquid at a uniform temperature, some of the ions in the material experience a force. This electrostatic force, F_{es}, arises because in any electric field, charges of opposite sign attract and charges of like sign repel one another. As the magnitude of the charge, Z, increases so does F_{es}.

The ionic mobility becomes

$$\mu_{es} = \frac{v_i}{Ze\vec{E}'} \tag{2}$$

where e is the electronic charge and $\vec{E}'$ is the electric field seen by the ion corrected for electronic shielding. $\vec{E}'$ is usually assumed to behave linearly with the applied field, $\vec{E}$. If F_i is the "diffusive" force, and the ion is only subjected to this and F_{es} during current flow, equations (1) and (2) can be combined to give the effective ionic mobility, μ_{eff}, as[23]

$$\mu_{eff} = \mu_o \frac{F_i}{Ze\vec{E}'} . \tag{3}$$

Since the ions in a metal typically give up an electron during conduction, these ions become positively charged. The electrostatic force, then, for electronic conductors would repel some of these ions from the anode and drive them to the cathode, i.e., F_{es} is in the direction of conventional current flow. In metals where hole conduction predominates, the polarity of F_{es} is reversed.[24]

Simultaneously, an electron (hole) wind force, F_{wd}, arises from the interaction of the moving electrons (holes) with the same ions in the material. As the electrons move, they encounter defects, including loosely bound metal ions along grain edges and grain surfaces, scatter, and in the process of this interaction, transfer their momentum to the ions. When conditions are such that this momentum exchange causes movement of an ion, this movement will oppose that due to F_{es} and be in the direction of actual electron (hole) flow.

To appreciate this electron-ion interaction, the electron's momentum must be examined. Without the field, the electrons have random motion with some electrons possessing a momentum, $\vec{p}_F$, such that

$$\vec{p}_F = (2m_e E_F)^{1/2} \tag{4}$$

where E_F is the Fermi energy of the metal and m_e is the electron's mass. With the application of an electric field, $\vec{E}$, only those electrons near the Fermi surface, i.e., those having momentum as described in equation (4), will be preferentially accelerated in the field direction with an additional momentum, $\Delta\vec{p}$, such that

$$\Delta\vec{p} = e\vec{E}' \frac{\ell}{v_e} \tag{5}$$

where ℓ is the mean free path of electrons in a perfect metal lattice and $\tau = \frac{\ell}{v_e}$ is the mean time between scattering events. It is assumed that such scattering events are elastic, in that the collision causes a change of direction with little change in energy. This assumption is reasonable since $\vec{p}_F > 10^7 \Delta\vec{p}$ for a typical gold film subjected to 1 Amp.[25]

By rewriting equation (5), the drift velocity of an electron induced by the applied field can be described by

$$v_e = - \frac{e\vec{E}'\tau}{m_e} \tag{6}$$

where the minus sign indicates flow from cathode to anode. The kinetic energy of the electron can now be written as

$$E_{KE} = \frac{e^2\vec{E}'^2\tau^2}{2m_e} \ . \tag{7}$$

If the electron looses some portion of its induced energy through events other than ionic scattering and it is assumed that ionic scattering is enhanced as the ion's charge increases, then the amount of energy transferred to the ions by the moving electrons is [26]

$$E_{wd} = Z\omega(\lambda\frac{e^2\vec{E}'^2\tau^2}{2m_e}) \tag{8}$$

where $\lambda \leq 1$.

Since E_{es} and E_{wd} serve to bias the ion motion, it is possible to write equations that describe the probability that an ion will move parallel to the applied field in the direction of the electron wind, f_{wd}, or in the opposite direction, f_{es}, such that[26]

$$f_{wd} = \beta\,\frac{\eta'}{\eta}\,\nu'\exp\{(-E_m - \frac{Ze\vec{E}'a}{2} + \frac{\lambda Z\omega E_{KE}}{2})/kT\} \tag{9}$$

and

$$f_{es} = \beta\,\frac{\eta'}{\eta}\,\nu'\exp\{(-E_m + \frac{Ze\vec{E}'a}{2} - \frac{\lambda Z\omega E_{KE}}{2})/kT\} \tag{10}$$

where β is a geometrical constant describing the lattice, η' is the number of vacancies per unit volume, η is the number of ions per cm^3 such that $\eta + \eta' = 1$, ν' is the vibrational frequency of the ion in the specimen, k is Boltzmann's constant and T is the absolute temperature. E_m is the lattice potential barrier height for diffusion. The average drift velocity of the ionic species is

$$\overline{v_i} = a(f_{es} - f_{wd}) \tag{11}$$

where a is the lattice spacing of the matrix. In order to get equation (11) in a form that contains tractable experimental variables, equation (9) and equation (10) can be substituted into equation (11). After suitable mathematical manipulation and further substitution of physical constants, S. T. Pai and J. P. Marton describe the average ionic drift velocity as [26]

$$\overline{v_i} = \frac{D}{kT} ZeE \left(\varepsilon - \psi \frac{(n_e{}^2 e^4 \tau^2)}{m_e{}^2} \rho\right) . \tag{12}$$

But

$$\rho = \frac{m_e}{n_e e^2 \tau} \tag{13}$$

giving

$$\overline{v_i} = \pm \frac{D}{kT} ZeE \left(\varepsilon - \psi/\rho\right) \tag{14}$$

as the average ionic drift velocity due to diffusion and electromigration in current-stressed electronic conductors. An examination of equation (14) indicates that the effective charge, Z*, of the ion is

$$Z^*_{P\&M} = \pm Z(\varepsilon - \psi/\rho) . \tag{15}$$

If hole conduction is included, then the general form of Z* is [26]

$$Z^*_{P\&M} = \pm Z_e(\varepsilon - \psi/\rho_e) \mp Z_h(\varepsilon - \psi/\rho_h) . \tag{16}$$

The EM flux can then be obtained by

$$\vec{J} = \overline{v_i}\, C(x,t) = \pm \left(\frac{\overline{C}D}{kT}\right) ZeE \left(\varepsilon - \psi/\rho\right) \tag{17}$$

if the concentration profile, C(x,t), of the ionic species can be obtained.

Due to the large number of material constants needed for evaluation of equations describing the EM effect as exemplified in equation (17), the majority of researchers have based the comparison of theory with specific experiment upon a value of Z* as described in equations similar to equation (15). The value and sign of Z* is considered a material constant that defines the degree of electromigration for a given metallurgical system and Z* is often rewritten in the form of an arithmetic sum of the two forces acting on the ion, i.e.,

$$Z^* = \pm Z^*_{es} \mp Z^*_{wd} = \pm Z\varepsilon \mp Z(\psi/\rho) \ . \tag{18}$$

H. B. Huntington and A. R. Grone[27] have developed a description for Z^*_{wd} such that

$$Z^*_{wd} = -Z \left(\frac{\rho_d}{N_d}\right) \left(\frac{N}{\rho}\right) \frac{|m^*|}{m^*} \tag{19}$$

where $\frac{\rho_d}{N_d}$ is the specific resistivity of the moving impurity ion, $\frac{N}{\rho}$ is the inverse specific resistivity of the lattice atom and $\frac{|m^*|}{m^*}$ is the corrected effective electron mass. If it is assumed that $Z^*_{es} = Z$,[28] an equation for Z* can be written as

$$Z^*_{H\&G} = \pm Z \left(1 - \left(\frac{\rho_d}{N_d}\right) \left(\frac{N}{\rho}\right) \frac{|m^*|}{m^*}\right) \tag{20}$$

which differs little in form from the original equation of V. B. Fiks for the same quantity,[23] namely,

$$Z^*_{FIKS} = (1 - n_e \ell \sigma^*_i) \tag{21}$$

where σ^*_i is the scattering cross-section for impurity ions and $\sigma^*_i > \sigma^*_{MATRIX} = \frac{1}{n_e \ell}$.

Current theoretical work centers on the application of quantum mechanical methods to the electromigration problem. These "polarization" models differ from the abovementioned "ballistic" approaches in that rather than considering the momentum transfer as a discrete collision, the moving electrons interact with localized ionic potentials that differ from matrix atom to impurity. While the final result of the Bosvieux-Friedel[29] model can be reduced to the ballistic Z* in equation (20), the authors remove the condition that the defects that are affected by electron flow are decoupled from the lattice. By assigning a dipolar charge to the defects/impurity ions in the matrix, the model can incorporate the effects of electron momentum transfer to the ions' surroundings, including vacancies. R. S. Sorbello[30,31] rigorously determines the electron charge density and allows the force due to this density to dissipate throughout the entire crystal rather than only the diffusing atom of interest. Other authors[32,33] continue the polarization charge models with the result for simple metals reducing to

$$Z^* = Z\ (1 - \frac{\Delta\rho}{N_d}\ (\frac{N}{\rho})) \tag{22}$$

where $\Delta\rho = \rho_d - \rho$.

2.3 Electromigration in Thin Films

In Section 2.2, a number of equations describing the electromigration process were introduced. The majority of these approaches are somewhat limited in that they were formulated to describe the EM process in bulk metal systems. As will become evident, most researchers have modified the equations that govern bulk electromigration to take into account thin film features.

2.3.1 Characteristics Specific to Thin Films

There are two primary differences between thin film and bulk systems. First, thin films have an enhanced surface-to-volume ratio when compared to their bulk counterparts. Second, all thin film properties are more sensitive to processing procedures than are bulk samples. Within these two categories, a number of secondary differences exist.

The high surface-to-volume ratio is a direct consequence of the thickness of the films produced. Typical films range in thickness from 100 Å to 50,000 Å. Such films must be deposited on some form of substrate to impart mechanical stability to the film.

During current passage, the substrate aids in heat dissipation due to the localized bonding at the film/substrate interface. This interface can also produce deleterious effects. Impurities in the processing environment or in the substrate itself can become trapped at this interface, coalesce and produce areas of non-adhesion causing local hot spots along the film. Current powering can cause these impurities to enter the film, diffuse throughout the specimen and reduce the film's electrical response or lower its resistance to corrosion. Differences in the thermal coefficients of the films and substrate can produce unwanted stress in the film during pulsed powering.

The film/environment interface takes on a major role in affecting thin film behavior as well. Impurity adsorption has been shown to have a dramatic effect in altering the surface diffusion of a number of metals commonly used to fabricate thin films. In the case of aluminum, where surface diffusion has a large impact on matter transport at room temperature, an overcoat of silica glass has been observed to cause an increase in the activation energy for electromigration.[20] C. A. Chang has shown that the film/environment interface activates an entirely different mechanism. In the case of Au, an oxidizing atmosphere stimulates the out-diffusion of Si from the substrate and Cr from certain intermetallic layers into the Au film[34] which affects the EM behavior of these films. The large amount of film surface exposed to the environment promotes increased oxidation/corrosion of certain films.

The most important effect of the large surface-to-volume ratio in thin films is the enhancement of grain boundary/surface diffusion due to the presence of a high degree of disorder along the film's two interfaces and grain edges. These are but a minor part of the overall volume of a bulk sample, and are often not considered as the primary locations for producing diffusion-related failure in a bulk specimen. This is not the case for thin films, where measurable rates of grain boundary diffusion in the film occur at room temperature, while appreciable bulk diffusion often requires temperatures close to the material's melting point.

With regard to electromigration, the determination that grain boundary diffusion controls the EM rate in a majority of thin film systems was qualitatively the most promising discovery needed to describe EM and therefore helped to explain certain microcircuit failures. J. R. Black[20] and recently, M. H. Fariàs et al.,[35] have shown for pure Al and K-doped Au thin films, respectively, that as grain size decreases, the grain boundary diffusion of Al in Al and K in Au increases. J. R. Black also demonstrated that as the grain size decreased, the median time for EM failure decreased.

Quantitatively, however, grain boundary diffusion has been difficult to monitor. Concentration profiles so produced are not amenable to bulk techniques. When appropriate methods for studying grain boundary diffusion are used, the amount of diffusant in the boundaries is often less than the detection limit of these methods and the variation of the diffusion coefficient as a function of local boundary orientation and impurity adsorption makes data collection and interpretation difficult. To date, even the nature of the grain boundary--its width, its structure and its ability to trap impurity atoms or to hold grain edge matrix atoms--is not easily understood, nor is the coupling between boundary and surface diffusion which varies from system to system.

Solute solubility in grain boundaries differs from bulk values, making assumptions of the initial impurity concentration difficult. Segregation coefficients for the common alloy systems have yet to be determined.

Finally, void coalescence leading to hole formation produces catastrophic failure in thin films, since such formations represent a much larger percentage of the sample's overall cross-section when compared to bulk samples.

The degree to which processing influences thin film properties cannot be overemphasized and has been demonstrated by J. C. Blair et al.[12] In their study, Au was vapor deposited on a SiO_2 substrate held at 200°C, to produce a film having an average grain diameter of 2000 Å. After an anneal of 450°C/24 hr, the grains grew to an average diameter of 11,000 Å, with a corresponding resistivity decrease from 2.67 μΩcm to the bulk value of 2.45 μΩcm. The researchers then produced Au films having the same average grain size by sputtering. In this case they found that the initial grain size varied little as a function of Ar sputtering pressure, but that the resistivity varied markedly. After the same anneal, the sputtered films showed no measurable grain growth, and, while their resistivities had dropped by 2.2-4.0 μΩcm, bulk resistivity values were never attained. Other property differences are acknowledged for the wide range of deposition techniques that span e-beam deposition, chemical vapor deposition and others.

Each technique has a variety of variables that affect the final product, including the source distance, the pressure and composition of the ambient, the voltage applied, the substrate temperature and polarity, etc. Substrate orientation and cleanliness can alter the nucleation and growth of the film and often determine the film's texture. Epitaxial growth can be stimulated by choosing a substrate whose structural features strongly parallel those of the film material or choosing ionic oxides such as NaCl or KCl as substrate materials.

All of these variables produce a thin film product that is far from the polycrystalline, isotropic, highly reproducible bulk specimen of the same material. These features make theoretical implications and experimental results highly individual to date and often not easy to relate to bulk data.

2.3.2 Brief Survey of Thin Film EM Models

Several mathematical expressions for thin film EM exist. Researchers have attempted to tailor bulk electromigration equations through the use of additional multiplicative terms. For example, P. S. Ho et al. have postulated that the flux along thin film grain boundaries due to EM can be written as[36]

$$J_{gb}^{EM} = \frac{\delta}{D} N_{gb} \frac{D_{gb}}{kT} Z^*_{gb} \, eE \qquad (23)$$

where δ is the average width of a grain boundary (often evaluated at 5 to 10 Å), D is the average grain diameter and N_{gb} is the defect concentration in the boundary which is assumed constant. Recalling equation (17) it is seen that equation (23) is simply equation (17) multiplied by the factor δ/D with a redefinition of N_{gb}. These factors reduce the EM flux in proportion to the decrease in the activated volume for grain boundary diffusion. N_{gb} could be replaced by $N_{gb}(x,t)$. It is appreciated that while the form of equation (23) appears straightforward, $N_{gb}(x,t)$ and D_{gb} are still difficult to obtain experimentally.

R. Rosenberg phenomenologically acknowledges the added importance of variation in local grain boundary structure by indicating that the flux due to electromigration at a triple point, J_{gb}^{EM}, is[37]

$$J_{gb}^{EM} = \frac{N_{gb}Z_{gb}^{*}\ eE}{kT}\ (\ \pm D_1\cos\theta_1 \mp D_2\cos\theta_2 \mp D_3\ \cos\theta_3\ ) \qquad (24)$$

where a positive flux implies flow into the triple point and θ is the angle between atom motion in the boundary and the direction of the applied $\vec{E}$. As equation (24) suggests, it is expected that diffusion rates should vary locally with grain boundary structure and orientation. No grain size dependence is noted as in equation (24).

S. T. Pai and J. P. Marton have developed an equation[26] to describe EM in metals where it is anticipated that several material constants within the equation change as a function of metallic system and form. After determining the compositional variation across an Al thin film after current passage according to[11]

$$\overline{C}(x,t) = \overline{C}_o\ \exp(-F'(x)t) \qquad (25)$$

the authors evaluate $F'(x)$ in order to extract the necessary EM parameters. While several constants are the same for a 1000 Å Al film and bulk Al, others such as the structure factor and the collisional frequency differ from 2 to 6 orders of magnitude as a function of material form. These latter variations are anticipated since thin films are known to contain far more defects/cm^3 than their bulk counterparts.

P. S. Ho and J. K. Howard,[38] K. L. Tai and M. Ohring[39] and P. S. Ho[40] develop models for thin film EM by returning to the general thermodynamic approach of treating electromigration as a forced diffusion process interacting with random diffusion due to Joule heating. P. S. Ho and J. K. Howard[38] apply the Fisher-type solution of G. Martin[41] to determine the time-dependent compositional change in a thin film boundary caused by the coupling of these two processes. These researchers were able to experimentally determine Z^*_{gb} and $K\delta D_{Cu-gb}$ for Cu in an Al film matrix by tracking the composition of the stripe after current stressing using the electron microprobe technique and an "inverted" cross-stripe sample configuration. The diffusion coefficient was determined independently by conducting isothermal annealing experiments on silmilar samples.

P. S. Ho[40] develops the composition profile for coupled grain boundary diffusion and electromigration for different levels of competition between grain boundary and lattice diffusion using R. T. Whipple's Fourier-Laplace transform solution.[42] Mathematical manipulation of the concentration profiles gives values for Z^*_{gb} and δD_{gb} for pure thin film systems.

CHAPTER 3
SPECIMEN PREPARATION

The gold films used throughout this study were produced from 99.999% pure Au wire using standard high vacuum practice and thermal evaporation techniques.

Pure gold films were deposited on optically flat high purity quartz slides (3.75 x 2.55 x 0.10 cm^3). Lack of impurity content in the quartz was verified by examination of the infrared spectrum for a representative slide.

Au films to be doped with Group IA impurities were deposited on high purity borosilicate ribbons,[43] each containing 7.5 mole% of the appropriate alkali metal oxide. Table 1 lists the specific composition of each glass type used. The average cross-sectional area of the ribbons was 0.36 x 0.01 cm^2.

The boron oxide, B_2O_3, is a required glass constituent which is needed to incorporate the network-modifying alkali elements into the silica matrix and thereby allow for the production of a uniform and usable substrate. (Without the addition of a network-former such as boron, a Na_2O-SiO_2 glass will dissolve overnight in water.[44])

All of the borosilicate surfaces were smooth, although some portions of the lithium borosilicate ribbon exhibited ridging due to the drawing process. Upon inspection, only the Li-borosilicate glass appeared somewhat opaque, indicating that some phase separation had

Table 1. Composition of Borosilicate Glasses
Used as Substrates for Alloyed Gold Films

	SP502		SP504		SP505	
	Mol.%	Wt.%	Mol.%	Wt.%	Mol.%	Wt.%
SiO_2	72.5	67.48	72.5	69.86	72.5	72.94
B_2O_3	20.0	21.57	20.0	22.33	20.0	23.31
LiO_2	--	--	--	--	7.5	3.75
Na_2O	--	--	7.5	7.81	--	--
K_2O	7.5	10.95	--	--	--	--

occurred during production. While this immiscibility persists on the micron level, such an effect would be inconsequential to the work reported here.[45]

Representative samples of each alkali glass were analyzed using Auger Electron Spectroscopy (AES) and were seen to have no crossover contamination. Each substrate type was isolated and stored in a desiccator held at 1 Torr until use.

Approximately one hour prior to deposition, a sufficient amount of substrate was removed from one of the desiccators and examined. Specimens that exhibited obvious ridging, scratches, seed, stone or bubble formation were discarded. The substrates were then ultrasonically cleaned in the following sequence:

1) Alconox detergent (7.3% phosphorous by weight, pH 9.0-9.5) and water--to remove water-soluble and some organic contaminants including oils, greases, soils and carbon products.[46]
2) MICRO™ and de-ionized water--to further remove water-soluble contaminants through the use of a higher grade detergent.
3) Reagent grade acetone--a semi-polar solvent acting as a vapor degreaser.
4) Reagent grade alchohol--a less polar solvent containing fewer inherent impurities used to continue the cleaning action initiated by the acetone wash.

The substrates were then subjected to a stream of dry air and re-examined optically for flaws. While several glass/ceramic specialists would contest the degree of rigor in the aforementioned cleaning regime,[47] a number of thin film researchers[48,49] follow similar cleaning procedures.

The substrates were then mounted in spring-loaded holders that enabled the placement of a molybdenum mask of the desired film pattern directly over the glass. The fabrication of the masks used in this study closely followed the photo-etch technique described by W. A. Slippy.[50] These holders were then placed in the vapor deposition vacuum chamber for film production.

After the appropriate substrates and source material were placed in the chamber, the system was immediately closed and the heating tapes surrounding the base of the chamber were disconnected. (Several heating tapes, rated at a maximum temperature of 450°C, were always fully activated prior to opening the vacuum system in order to minimize impurity adsorption along the walls and constituent parts of the chamber.) A mechanical pump was used to bring the pressure in the chamber to 150-200 μm (.15-.20 Torr) within 3 to 5 minutes. This cut-off pressure and the use of a zeolite-filled sorption trap minimized the backstreaming of water and hydrocarbon molecules from the mechanical pump oil back into the chamber. Laboratory grade nitrogen was then bled into the chamber to a maximum pressure of 2000 μm (2.0 Torr) to reduce the partial pressure of oxygen and water vapor. This process was repeated several times, each time bringing the overall pressure down to 150-200 μm (.15-.20 Torr). A liquid N_2-cooled adsorption pump then reduced the overall pressure to 1-5 μm ($1-5 \times 10^{-3}$ Torr) by particularly reducing the partial pressures of nitrogen, carbon dioxide, water vapor and residual hydrocarbons. After outgassing the titanium filaments of an Ultek 224-0610 sublimation pump, the adsorption pump was closed off.

Two sputter-ion pumps, in conjunction with the sublimation pump, brought the system pressure down to the deposition pressure typically within 1-3 hours. Base pressures prior to deposition were in the range of 6-20 x 10^{-8} Torr.

The Au was evaporated from a Mo or W boat that was resistively heated by 180-183 Amps generated by an Ultek model 60-305 kV power supply. Sufficient Au wire was used to prevent any that evaporated from wetting the boat surface. Deposition rates--being a function of the surrounding pressure, heating current and boat material--varied from 2.3 Å/s to 12.6 Å/s with an average rate of approximately 4.0 Å/s.

Upon completion of the deposition, the samples were removed from the vacuum chamber and inspected with an optical microscope at 30X magnification. The critical film dimensions were $1.65 \times 0.15 \times 800 \cdot 10^{-6}$ cm^3. Films possessing pinholes, scratches, irregular pattern delineation, surface marks or notable contamination were discarded.

The thicknesses for all samples, unless specifically stated, were within 800 ± 10 Å, as measured in situ with a Granville-Phillips 0-01-219016 piezoelectric film thickness monitor calibrated for gold. Several samples were randomly chosen and examined with a Sloan M-100 optical interferometer. Their thickness values as determined by the quartz monitor were well within the experimental error attributed to the interferometer.

CHAPTER 4
TEMPERATURE-INDUCED SURFACE CHANGES IN GOLD THIN FILMS

4.1 Observation of Parallel Degradation Processes During Current Passage

Preliminary electromigration experiments indicated a marked contrast in the observed failure location of pure gold films when compared with that of gold films deposited on an intermediate adhesion layer of 135 Å of indium. (These studies are described in detail in the appendix.) The results of this work verified that several parallel processes occur in a thin film system during dc powering, and that the process that eventually produces failure can change as a function of film composition and experimental conditions. For example, for a given experimental procedure, in which a ceramic sample holder is used during dc stressing, pure 800 Å Au films fail by grain boundary grooving, while 800 Å Au films deposited on an intermediate layer of indium fail by electromigration. Because of these different mechanisms, failure in pure Au is located in the central portion of the metallization, while failure in In-doped Au is relegated to the cathode region of the stripe. By replacing the ceramic substrate holder with one of metal the overall film temperature during current stressing was reduced. This enabled EM to be the primary failure mechanism for all film compositions examined here.

While the major impetus for this research was an analysis of the effect of dopant on the EM behavior of gold, particularly an explanation of the "reversal" of electromigration failure site in Na-doped

Au,[1] it became apparent that solutes could affect a broader range of processes that are caused by the elevated temperatures induced by dc stressing.

A systematic study of these thermally-activated processes, in addition to electromigration, was undertaken in order to define the effect of dopant on the overall degradation of thin gold films subjected to direct current flow.

4.2 Annealing Behavior of Pure and Alloyed Gold Films

In order to more fully appreciate the degree to which alkali outdiffusion might affect the grain boundary grooving of gold thin films during resistive heating, an isothermal annealing study was conducted. Of primary interest was whether grain boundary grooving could compete with electromigration as a failure mechanism and whether the degree of grooving was a function of solute. Such an annealing study offers insight into the behavior of solutes in gold at elevated temperatures with no driving force other than that of a difference in the chemical potential between the solute in the film's substrate and the solute at the film's free surface.

The annealing study was carried out in two parts. The first group--pure Au, Na-doped Au and In-doped Au--allowed for the characterization of grain boundary grooving as a function of solute and method of solute introduction. The second study--Li-doped Au, Na-doped Au and K-doped Au--focused on the varying degree of grain boundary grooving as a function of Group IA impurity.

All samples were annealed in a Lindberg type 54457, 3-zone, tube furnace. Annealing times and temperatures were consistent within the two parts. The temperatures were chosen to approximate those produced along the stripe during the EM test. These temperatures were measured by correlating the substrate temperature adjacent to a test stripe with the initial melting of metal chips ($T_M \leq 420^oC$) placed directly on the test stripe after incremental changes in the applied current. The annealing temperatures were that of the stripe adjacent to the electrode during 1 Amp powering ($190\text{-}200^oC$), that of the center of the stripe during 1 Amp powering ($340\text{-}350^oC$), and a higher temperature ($500\text{-}560^oC$) to accelerate any thermally-activated processes. All samples were deposited along with samples used for EM testing and were identical in form and prior history.

The first group of isothermally annealed samples (Figures 1 through 3) depict films heated under a pressure of 1 Torr. Each figure describes the behavior of a single composition, with the temperature increasing from 25^oC to 560^oC from left to right. The SEM micrograph magnifications increase from top to bottom. Sample preparation for data acquisition with the SEM will be described elsewhere (Section 5.2).

Pure Au films deposited on high purity quartz slides are depicted in Figure 1. Au films deposited on Na (microscope) glass are shown in Figure 2. Earlier Auger analysis had shown appreciable diffusion of Na from common microscope slide to the gold surface after 5 minutes at 100^oC.

Figure 3 depicts results for In-doped gold, where the indium was introduced into the film by way of a pure 135 Å In film sandwiched between the Au film and the quartz substrate. The electrode/boat configuration for the vapor deposition of these samples was designed to permit consecutive depositions of In and Au without breaking the vacuum.

The contrast in the Au thin film surface as a function of dopant and dopant source is extensive for the three systems shown here.

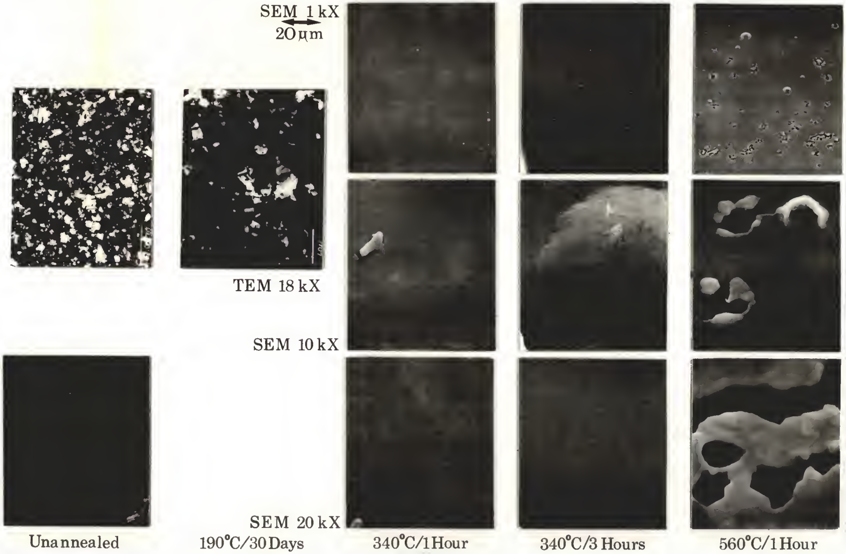

Figure 1. Annealing Behavior of Pure Gold Thin Films (Quartz Substrates).

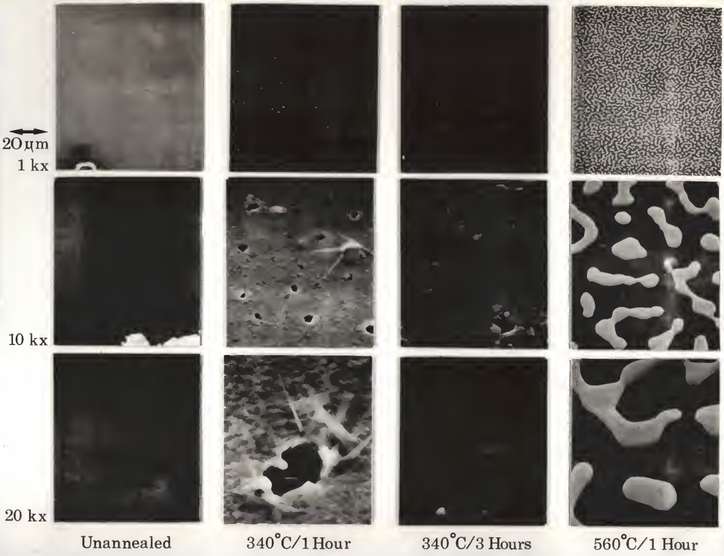

Figure 2. Annealing Behavior of Gold Thin Films (Na-Glass Substrates).

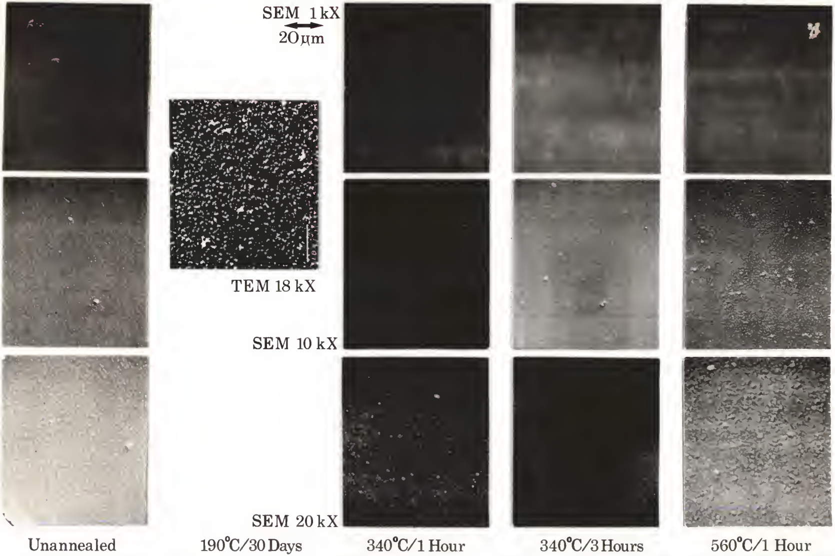

Figure 3. Annealing Behavior of Gold Thin Films (135 Å Intermediate Indium Layers on Quartz Substrates).

The surface of pure gold (Figure 1) remains unaffected by thermally-induced surface tension changes until some time after 1 hour at 340°C. Detectable, uniform grain boundary grooving is visible after 340°C/3 hr at 20kX magnification. The lack of severe grooving and associated surface roughening may in part be due to O_2 adsorption on the pure gold surface, which is known to occur even at UHV pressures and temperatures close to the melting point of gold.[51] O_2 adsorbates decelerate Au surface diffusion as measured by reduced thermal grooving and marker motion in contrast to Cu and Ag.[52] Some blisters are visible throughout the stripe, but they are most likely caused by atmospheric impurities that were trapped at the Au/quartz interface during processing.

Hole formation due to prolonged grain boundary grooving is not visible in pure gold films until an annealing regime of 560°C/1 hr. The holes vary in shape. Some are equiaxed and have areas comparable to the film's grain size, while others are elongated and have areas equaling several grain diameters. In all cases the hole edges are faceted and show localized film thickening immediately adjacent to the hole. No surface roughening is noted in areas that contain no holes or blisters.

In contrast, Na-doped gold (Figure 2) shows substantial surface roughening and some hole formation due to grain boundary grooving after only 1 hour at 340°C. The holes, while still faceted, remain moderately equiaxed when compared with those formed in pure Au at the higher temperatures. Longer annealing times at 340°C cause the production of a higher density of holes, and while larger, they remain equiaxed.

The most noticeable effect seen in Na-doped Au is the complete destruction of film continuity at the highest temperature used in this work. As much as 70%[53] of the glass substrate is no longer covered with Au after 560°C/1 hr. The gold islands left on the sodium glass are either small, single-grained and equiaxed or elongated and contain several grains lined end to end. The islands are not faceted. Grain sliding alongside the holes does not appear in the Na-doped samples as it did in the pure Au specimens.

In-doped Au films experienced completely different behavior upon annealing than either pure Au or Na-doped Au films. As the SEM micrographs in Figure 3 indicate, the Au grains are much smaller and the surface somewhat rougher in the initial, unannealed condition. (The average grain size of the unannealed Au films deposited on the In underlayers is 0.05 μm, while the same for Au on quartz is 0.20 μm.) The surface does not change appreciably throughout the entire annealing schedule. While grain boundary grooving may have been enhanced after 560°C/1 hr, not only is it slight, but the annealing process produces no observable hole growth at any point throughout the annealing study.

4.3 Annealing Behavior of Gold Films Due to Alkali Additions

The second part of the isothermal annealing study was conducted to isolate the effects of alkali additions on the behavior of Au films subjected to elevated temperatures. The information gathered here was used in conjunction with that collected during electromigration testing. While the sample preparation, annealing procedure and SEM analysis were identical to that used for the first annealing study, two major differences were evident.

First, all samples were deposited on 7.5 M_2O-20.0 B_2O_3-72.5 SiO_2 ribbons, where M = Li, Na or K. This enabled the analysis of structural changes in the films due to annealing to be based upon compositional differences. This is in contrast to the first annealing study in which film surface changes were due to both composition and to variations in dopant source.

Second, the samples were placed in clean, covered quartz petri dishes and annealed at atmospheric pressure rather than at 1 Torr. This regime more closely approximated typical EM testing conditions.

The results are depicted in Figures 4 through 6. The format is similar to that used to portray the first annealing study. Transmission optical micrographs (30X magnification) have, however, been added to show macroscopic effects. SEM micrograph magnifications increase from top to bottom.

In Figure 4, the results for 800 Å thin gold films deposited on lithium borosilicate glass ribbons are shown. Pinholes are apparent at 10kX after room temperature aging for approximately 51 days. These pinholes are not observed in unannealed pure Au films or similar as-deposited Au films on Na- or K-borosilicate glass.

Isolated hole formation and overall surface roughening are not apparent until 350°C/5 hr. The holes pictured here are faceted, moderately equiaxed and have surface areas containing several grain diameters. Localized thickening adjacent to the hole is observed at 10kX. While the hole size and density are enhanced in the Li-doped films after 500°C, the overall film surface is quite similar to that due to an anneal of 350°C/5 hr. Grains not associated with holes are more faceted, however, than their counterparts at lower annealing temperatures. Localized film thickening near the holes persists. The degree

Figure 4. Annealing Behavior of Gold Thin Films (Lithium Borosilicate Substrates).

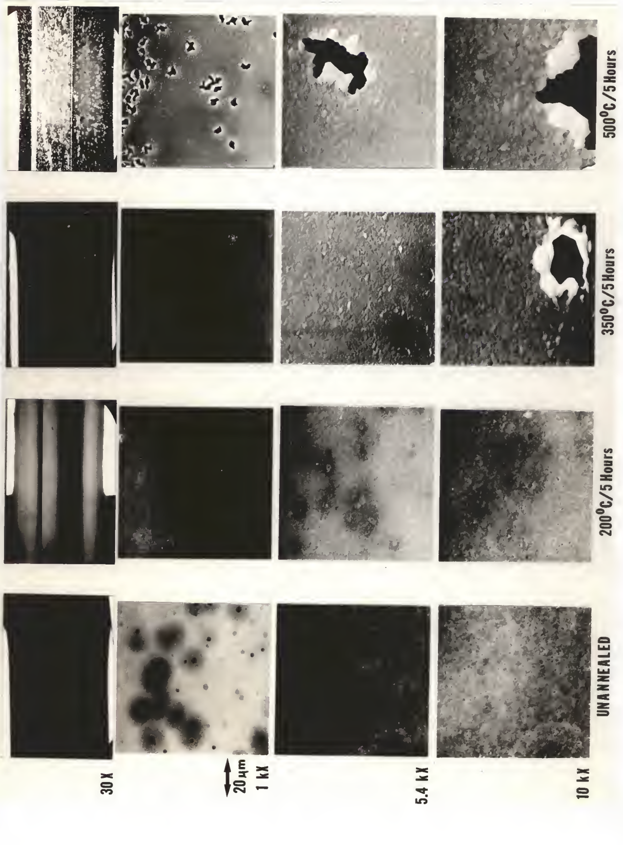
30 X
20 µm
1 kX
5.4 kX
10 kX
UNANNEALED
200°C/5 Hours
350°C/5 Hours
500°C/5 Hours

Figure 5. Annealing Behavior of Gold Thin Films (Sodium Borosilicate Substrates).

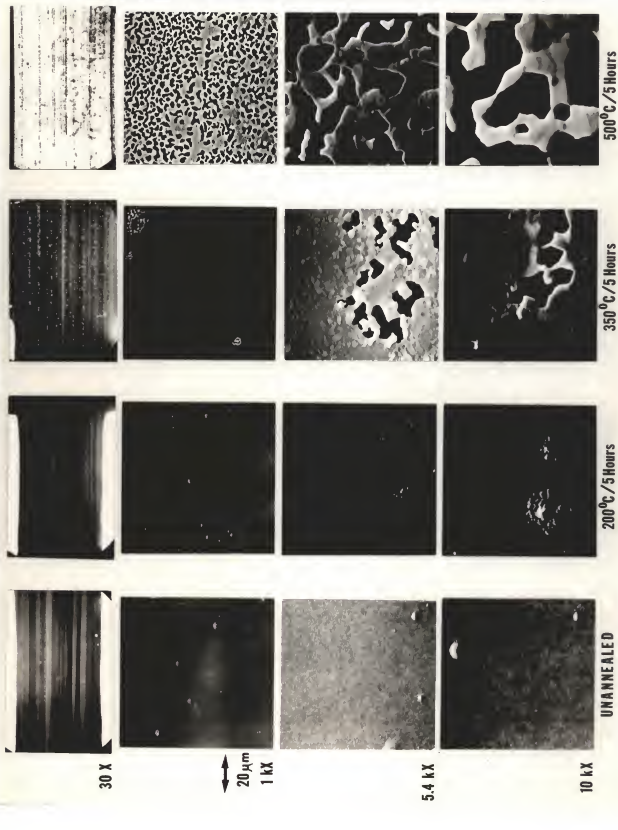
30 X
20 μm
1 kX
5.4 kX
10 kX
UNANNEALED
200°C/5 Hours
350°C/5 Hours
500°C/5 Hours

Figure 6. Annealing Behavior of Gold Thin Films (Potassium Borosilicate Substrates).

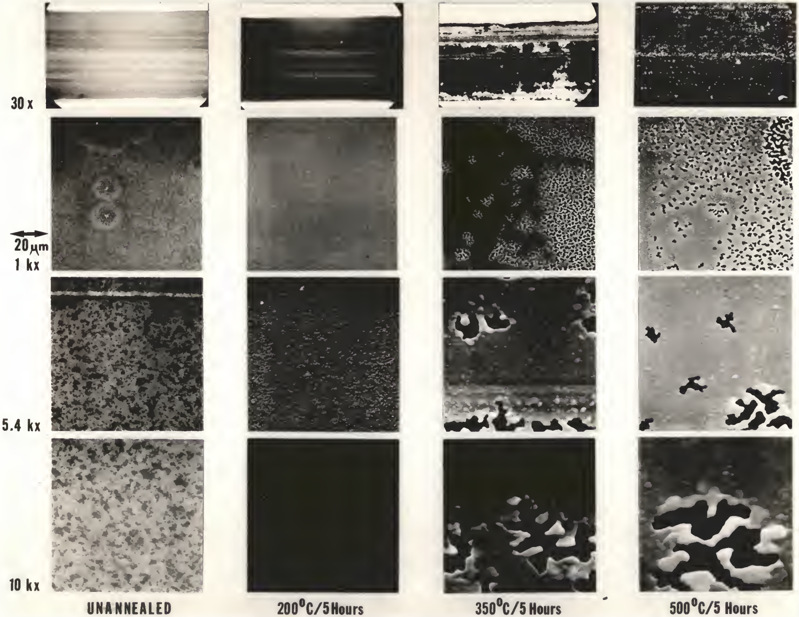
30 x
20 μm
1 kx
5.4 kx
10 kx
UNANNEALED
200°C/5Hours
350°C/5 Hours
500°C/5 Hours

of hole formation throughout the sample and therefore, diffusant introduction, does not appear uniform as indicated in the 30X micrographs.

The SEM data for Au films on Na-borosilicate glasses are collected in Figure 5. Little surface structure is visible at all magnifications for unannealed films and films subjected to $200^oC/5$ hr. Some minor hillocks are visible, but these are not typical. Rather severe hole formation and surface roughening occur after $350^oC/5$ hr. When compared to the Li-doped samples, the holes are elongated and of higher density. There is some localized film thickening alongside the holes, but not to the extent seen in the Li-doped samples. Surface roughening throughout the stripe is far more pronounced, as indicated in the 10 kX micrograph.

The most dramatic evidence of Au film degradation due to Na contamination is observed after an anneal of $500^oC/5$ hr. A marked increase in hole density and size is evident. The holes are an order of magnitude larger than the film's average grain size and their faceting is extremely sharp. The film maintains continuity but, as evidenced in the 30X micrograph, the hole volume is 60-70%[53] of the entire film.

Au films deposited on Na (microscope) slides annealed at 1 Torr can be compared with Au films deposited on high purity Na-borosilicate ribbons heat treated at 760 Torr (Figure 5). At 1 Torr, equiaxed holes are formed after $340^oC/1$ hr. Elongated holes form for the Na-doped samples at 760 Torr annealed at a similar temperature but for longer time. Surface roughening and grain pile-up are more pronounced for these latter samples as well.

At the maximum temperature and at 1 Torr, the Na-doped films are wholly discontinuous and the Au islands that remain possess rounded edges. These islands typically contain several grains connected on edge. After 500^{o}C/5 hr, the Au films deposited on Na-borosilicate substrates remain continuous with individual grain boundaries well delineated and the grains more faceted than in the first Na-doped group. In addition, the film areas have widths of several grains in contrast to the microscope slide films.

Finally, in Figure 6, the data for Au films deposited on potassium borosilicate glass are presented. As was the case with Au on Na-borosilicate, only slight surface roughening is apparent after 200^{o}C/5 hr. The hole configuration after 350^{o}C/5 hr is similar to that observed for Au on Na-borosilicate. The holes are irregular in shape and show grain pile-up nearby. Little has changed after 500^{o}C/5 hr, in contrast to the Na-doped samples. While the hole density has increased, the hole size and shape and degree of surface roughening are all comparable to that seen in the lower 350^{o}C/5 hr anneal. Some holes show no grain pile-up.

While it appears that the degree of grain boundary grooving (and associated hole formation) is least severe for Li-doped Au and most severe for Na-doped Au, several uncertainties exist which make such a determination premature. Li may produce the least Au film degradation because, being soluble in Au[54] (in contrast to Na and K), minimal amounts of Li may line the Au grain boundaries. In addition, since the Li-borosilicate glasses used were specifically prone to phase separation (See Chapter 3), Li mobility in the glass may be restricted. Finally, grain boundary diffusion rates for the alkali elements in Au are presently unavailable. Such metallurgical concerns must be addressed prior to specifying the degree of grain boundary grooving as a function of the alkali element introduced.

CHAPTER 5

ELECTROMIGRATION-INDUCED STRUCTURAL CHANGES IN GOLD THIN FILMS DUE TO ALKALI ADDITIONS

5.1 General Electromigration Test Conditions

Quartz slides and borosilicate ribbons, onto which were deposited 800-1000 Å Au films, were mounted onto metal substrate holders. The samples were placed in a straightforward dc circuit for EM stressing in the laboratory atmosphere. Constant current power supplies[55] were used. The voltage drop across each sample was monitored with a strip chart recorder[56] and was checked periodically through the use of additional multimeter measurements. While the value of the current passing through each sample was extrapolated by the change in resistance noted during instantaneous voltage increases and decreases, the current was also measured by means of an ammeter or amp-hour meter placed in series with the sample. Additional resistance measurements were made before and after the electromigration test. Upon removal from the circuit, each sample was prepared for SEM or AES examination.

5.2 Scanning Electron Microscope Results and Analysis

Several as-deposited samples were prepared to test whether an additional sample overlayer could improve signal resolution and inhibit sample charging caused by the glass substrate. SEM parameters were varied as well in order to optimize the black and white image recorded by the instrument.[57] Optimum SEM picture quality was attained through the use of

a) an additional 50-100 Å vapor deposited Al coating,

b) an accelerating voltage of 25 keV,

c) a working distance of 15 mm,

d) a 35° angle between the detector axis and sample surface, and

e) a 200 μm aperture.

The beam current varied due to W filament wear, but after alignment was typically 60 μAmps $\leq I_{beam} \leq$ 90 μAmps. In some cases, 30X optical micrographs were taken prior to SEM examination to catalogue macroscopic film damage.

Examples of the surfaces of dc-stressed pure Au films on quartz substrates are portrayed in Figures 7 and 8. In these figures, and in all subsequent figures in this section, areas of SEM examination are indicated in the accompanying schematic of the film. The physical characteristics for all samples discussed here appear in Table 2.

The pure Au films presented here lack excessive contamination and exhibit minimal surface features. Some pinholes, no larger than 0.5 μm, are evident across a large portion of the length of the sample depicted in Figure 7. The most prominent grain delineation and highest pinhole density is located near the cathode. These features decrease in density as the center of the film is approached until a clean, hole-free surface is observed near the anode. The uniform distribution of these features indicates that their formation is expected to be based upon the combined effects of localized EM material transport and thermally-induced grain surface readjustment at high energy grain edges and triple points.

The SEM micrographs in Figure 8 show that the sample half-length near the cathode surface is uniformly covered by small, elongated holes,

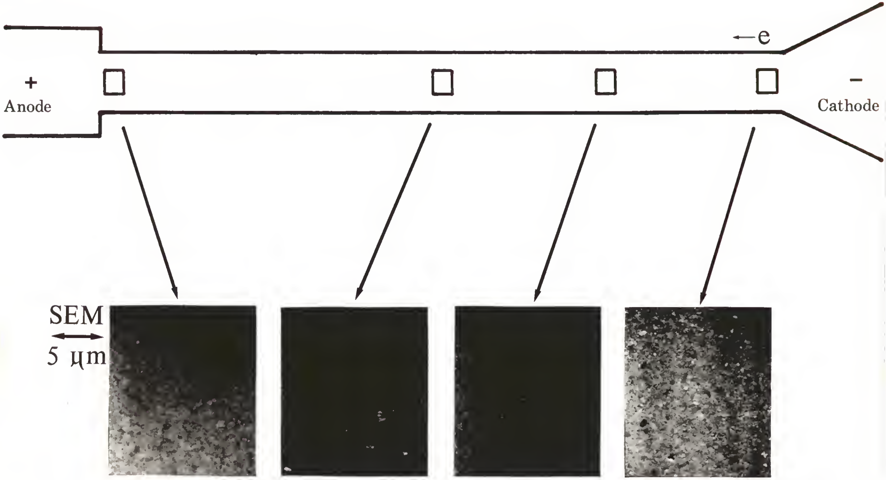

Figure 7. Pure 870 Å Gold Film Surface Following Current Passage of 7.53×10^5 Amps/cm^2 for More Than 2200 Hours.

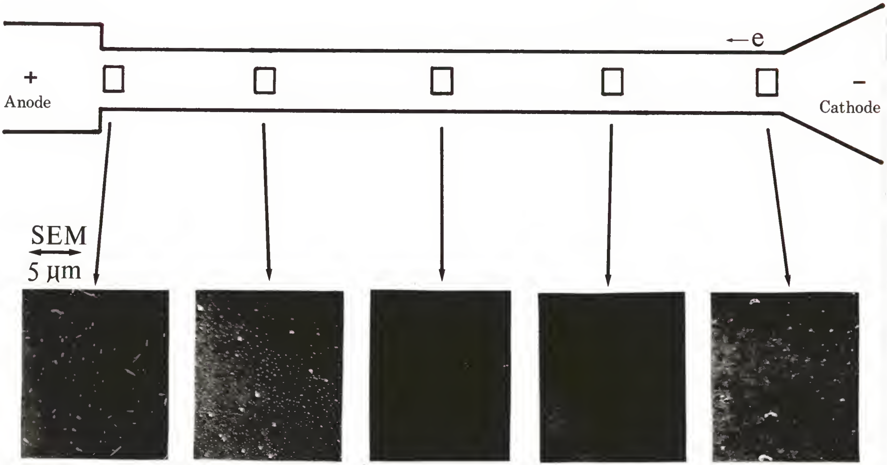

Figure 8. Pure 1000 Å Gold Film Surface Following Current Passage of 6.09×10^5 Amps/cm^2 for More Than 2200 Hours.

Table 2. Physical Characteristics and Test Conditions for Gold Films Used in SEM Study of Electromigration

Sample Number	GAu34C	GAu31B	GAuLi103E	GAuLi103D	GAuLi106A
Figure (In Text)	7	8	9	10	11
Thickness (Å)	870	1000	800	800	810
Initial Deposition Pressure (10^{-8} Torr)	6.0	15.0	7.0	7.0	3.0
Deposition Rate (Å/s)	NA [a]	9.2	3.4	3.4	9.8
Initial Resistance (Ω)	5.00	4.35	7.70	5.85	4.90
Final Resistance (Ω)	4.82	3.20	NA	NA	∞
Failure (Position along Stripe) [b]	None	None	None	None	60%
$\overline{J}$ (10^5 Amps/cm^2)	7.53	6.09	4.14	7.35	9.40
Length of Run (hr)	2262	2273	192	633	562

a) Not available

b) Failure across the length of the stripe is designated as a percentage of the total length, with the anode/stripe boundary assigned 0% and the cathode/stripe boundary assigned 100%.

Table 2 (continued). Physical Characteristics and Test Conditions for Gold Films Used in SEM Study of Electromigration

Sample Number	GAuNa104C	GAuNa109A	GAuNa108E	GAuNa108C	GAuK101C	GAuK105C
Figure (In Text)	12	13	14	15	16	17
Thickness (Å)	800	800	810	810	800	800
Initial Deposition Pressure (10^{-8} Torr)	2.2	10.0	5.5	5.5	1.8	8.0
Deposition Rate (Å/s)	2.9	6.8	10.7	10.7	3.8	9.2
Initial Resistance (Ω)	5.6	5.80	7.30	4.60	5.02	5.50
Final Resistance (Ω)	∞	∞	∞	NA a)	5.60	∞
Failure (Position along Stripe) b)	100%	69%	91%	None	None	16%
$\overline{J}$ (10^5 Amps/cm^2)	8.74	8.95	8.58	5.37	4.51	5.44
Length of Run (hr)	115	246	539	478	276	41

a) Not available

b) Failure across the length of the stripe is designated as a percentage of the total length, with the anode/stripe boundary assigned 0% and the cathode/stripe boundary assigned 100%.

in contrast to the previous pure Au film. These irregular, approximately 1 μm long holes are typical for EM-induced migration at local structural sites such as triple points. In the anode region, a number of smaller holes are seen to have adjacent material build-up.

The assymetrical location of grain delineation and pinhole formation (Figure 7) and larger hole formation (Figure 8) in the cathode portion of these two pure Au films is evidence of film damage due to electron wind-induced electromigration. As described earlier, grain boundary atoms are swept along the direction of electron flow, with material depletion occurring at the cathode and material accumulation at the anode. The surfaces of these two films indicate that these films were removed in the early stages of the EM process, with material depletion at the cathode--due to the combined effects of EM and slight grain readjustment--more prominent than measurable material accumulation at the anode. Both films resisted excessive EM-induced damage after dc stressing of 6.09-7.53 x 10^5 Amps/cm^2 for more than 2200 hours.

The SEM micrographs depicting Li-doped Au are shown in Figures 9 through 11. Optical transmission micrographs (30X magnification) of various film sections are also included in these figures. The samples in Figures 9 and 10 were removed prior to failure. All three Li-doped films exhibit severe grain boundary grooving, surface roughening and large hole formation in the two regions examined adjacent to the anode when compared with pure Au films stressed with comparable current densities. The optical micrographs reiterate these SEM observations. These lithium-doped samples were stressed for only one-tenth to one-fourth of the time that the pure Au films were stressed (See Table 2).

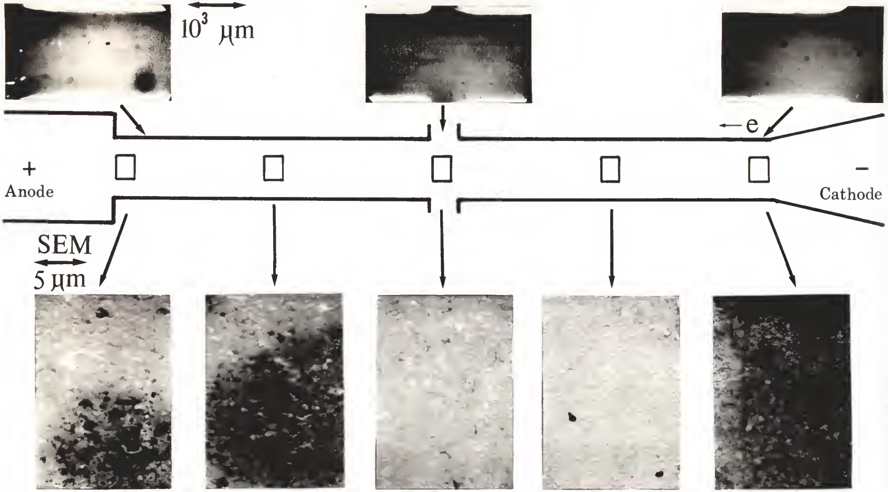

Figure 9. Electromigration Damage Along 800 Å Gold Thin Film Surface (Lithium Borosilicate Substrate).

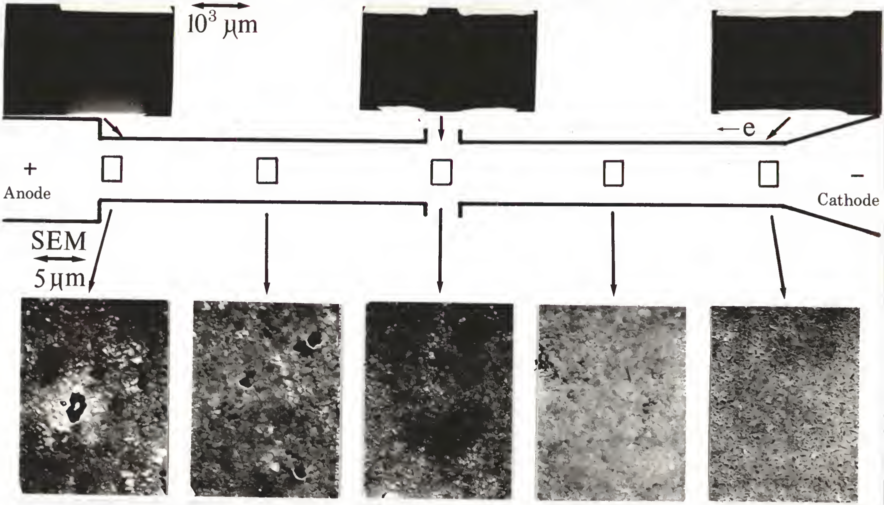

Figure 10. Electromigration Damage Along 800 Å Gold Thin Film Surface (Lithium Bobsilicate Substrate).

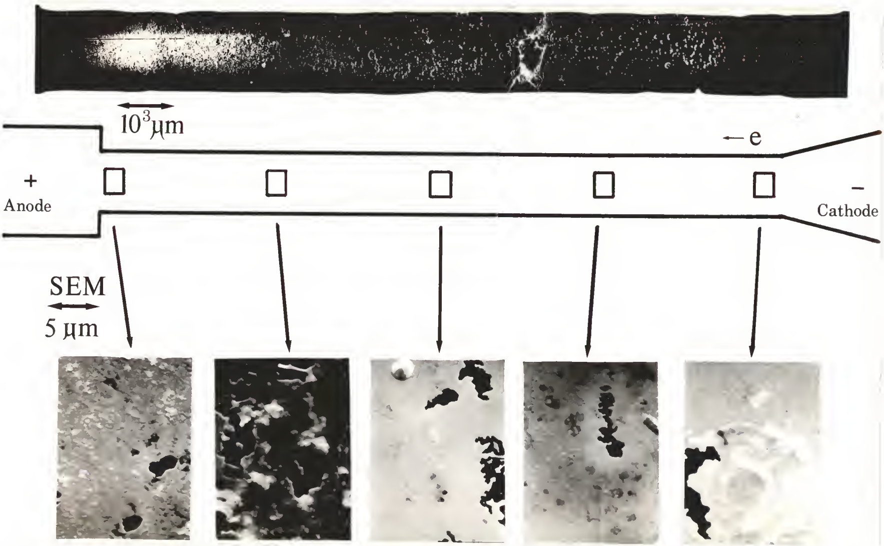

Figure 11. Electromigration Damage Along 810 Å Gold Thin Film Surface (Lithium Borosilicate Substrate).

The sample in Figure 9 shows well defined surface grain structure likely due to the alkali-enhanced grooving process at the center of the stripe, with enhanced boundary delineation, hole formation and alkali surface contamination as the anode region is approached. The holes seen are larger than the average grain size of the film and are faceted. Far less surface roughening is observed near the cathode portion of the stripe. Some pinholes are visible at the cathode area and are probably due to EM-induced Au depletion.

Similar behavior is noted for the Li-doped sample in Figure 10. The 30X photomicrograph of the anode verifies that the highest hole density occurs at the anode. Grain boundary outlines are more severe in this sample and persist throughout most of this sample. This is due to the stressing conditions, i.e., the current density and length of stress were greater by a factor of two and three, respectively, than for the sample depicted in Figure 9 (See Table 2). The character of the holes at the anode parallels that of the previous Li-doped sample, for the holes remain faceted and possess diameters larger than the grains themselves. The cathode portion of this sample exhibits no observable hole formation. The surface growths seen here were not noted in any other sample examined throughout this work and remain anomalous.

The final example of the surface of a Li-doped Au film subjected to dc stressing is shown in Figure 11. This sample was stressed at 9.40×10^5 Amps/cm^2 for 562.20 hours to failure. The 30X photomicrograph of this sample exemplifies the difficulty in basing EM reliability data on MTF (Median Time to Failure) studies. As the micrograph indicates, the sample developed an opening near the center of the film which prevented current flow. The dense ellipse of holes at the anode, however, is also evident and film failure at the anode--as in Figures 9 and 10--is competitive. The accompanying SEM micrographs show grain boundary grooving and hole formation at the anode portion of the stripe, similar to that shown in the previous two figures. The holes are much larger in this case but are identical in nature to those seen previously. The central and cathode portions of this film possess larger holes that correspond to the actual failure in the above photomicrograph, but these holes show no similarities with those seen at the anode. The cause of failure in this case is not precisely known although this latter hole formation is associated with areas of de-adhesion (See SEM micrograph of cathode region).

The effect of dc stressing on the surface of Na-doped Au thin films is shown in Figures 12 through 15. It is within this series that the variation in failure site location, for film samples of the same composition and similar stressing conditions, was first noted. Failures in Na-doped Au films occurred either near the anode or near the cathode. The surface features associated with each failure location were distinct. The Na-doped samples in Figures 12, 13 and 14 were all stressed at approximately 8.6-9.0 x 10^5 Amps/cm^2, while their times to failure increased from 114.9 hours to 245.8 hours to 539.4 hours, respectively.

The 30X optical photographs for the Na-doped sample in Figure 12 show that the film is macroscopically continuous near the anode and that failure occurred very close to the cathode. SEM micrographs reiterate this observation, depicting small (0.6-0.9 μm), equiaxed holes near the anode that are visible only at high magnification. The anode surface in this sample is identical to that produced by the isothermal annealing of a gold film on Na-microscope slide at 340^{o}C/1 hr (See

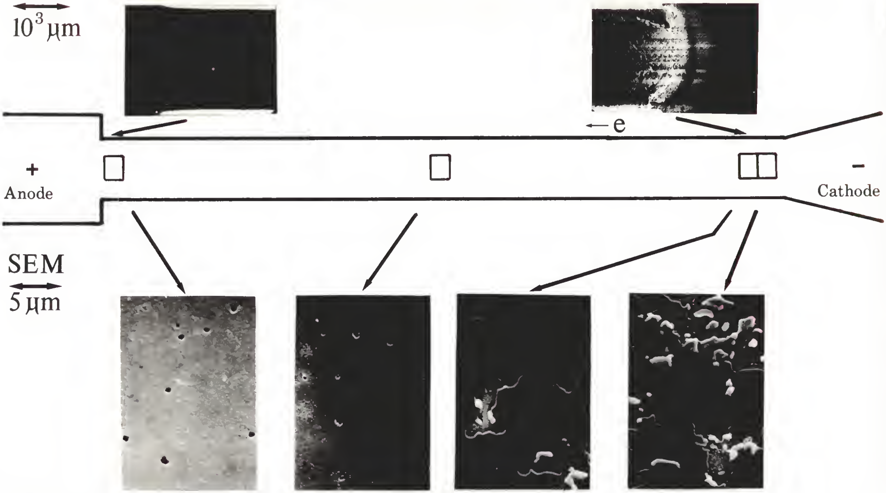

Figure 12. Electromigration Failure of 800 Å Gold Thin Film (Sodium Borosilicate Substrate).

Figure 13. Low Magnification (30X) Micrograph of Current-Stressed 800 Å Gold Thin Film (Sodium Borosilicate Substrate).

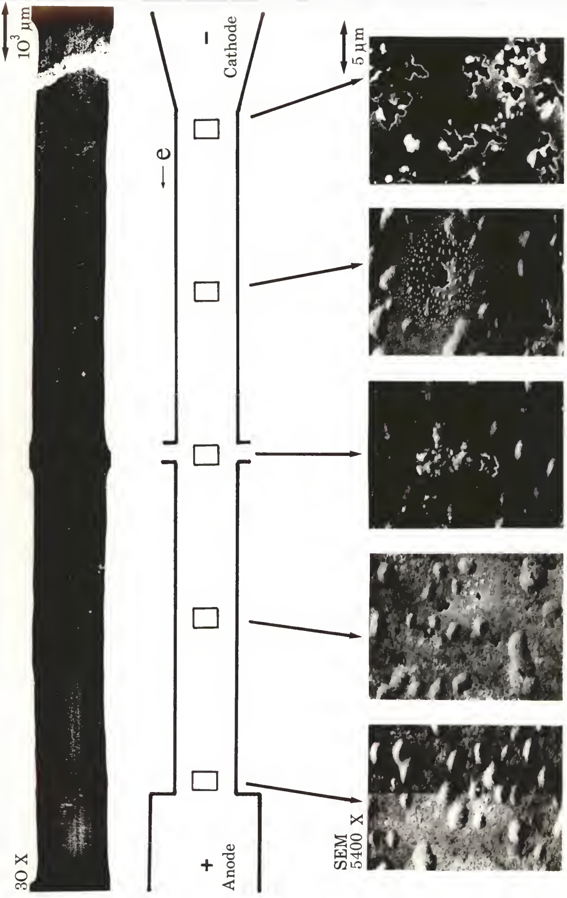

Figure 14. Electromigration Failure of 810 Å Gold Thin Film (Sodium Borosilicate Substrate).

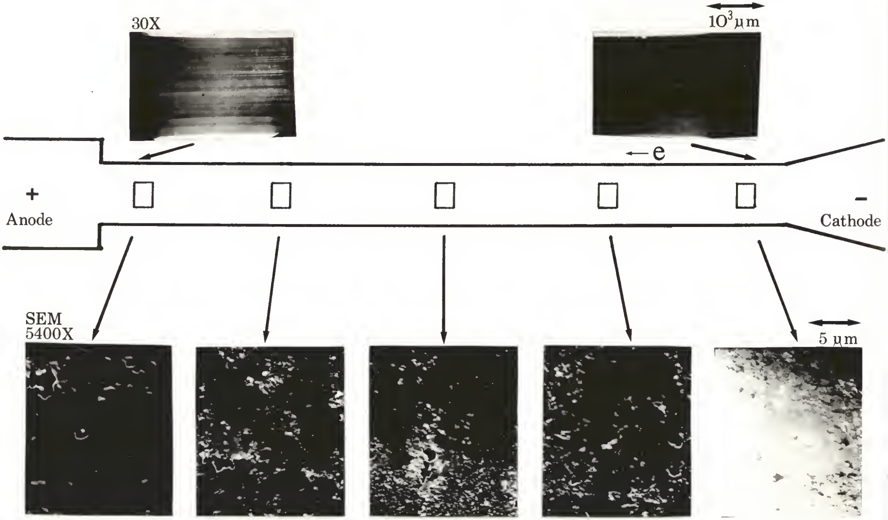

Figure 15. Electromigration Damage Along 810 Å Gold Thin Film Surface (Sodium Borosilicate Substrate).

Figure 2). The cathode region is seen to contain large irregularly shaped holes that typify Au electromigration failure. Some of these holes indicate the presence of local flux divergences due to non-uniform film microstructure in that hillock formation is immediately adjacent to the holes so formed. Some holes show no material build-up, indicating possible long range temperature gradient effects. Ultimate failure appears to be due to Au depletion at the cathode.

The Na-doped Au sample depicted in Figure 13 bears remarkable similarity to the Li-doped sample described in Figure 11. While the sample failed in a more central location, dense hole formation is observed at the anode, identical to the Li-doped film. The final failure is possibly due to de-adhesion in a manner similar to the Li-doped sample.

The optical micrograph in Figure 14 shows final failure due to an open in the extreme cathode region of the film as was seen in Figure 12. As was observed previously, an additional high hole density at the anode is also present. The accompanying SEM micrographs indicated surface roughening and extensive film de-adhesion along most of the stripe. Grain boundary grooving features including pinholes, grain boundary demarcation and faceted holes comparable to or larger than the film's average grain size are noted throughout most of the film. While pinholes are visible in the extreme cathode region, more apparent are the large EM-induced holes that penetrate the film. These holes, with or without adjacent material build-up are identical to those along the cathode surface in the Na-doped sample of Figure 12. This sample, which was stressed at nearly the same current density as the one depicted in Figure 12 but for a time length five times longer (See Table 2), shows far more surface roughening along the entire stripe than the earlier Na-contaminated sample. Ultimate failure arose due to Au depletion at the cathode.

Figure 15 is presented as a final example of Na's effect on thin Au films during dc stressing. The 30X photograph of the anode region shows hole formation while the cathode portion remains wholly continuous. This sample was removed prior to failure after being stressed at a 40% lower current density than the other Na-doped samples presented here. At higher magnification, severe grain boundary grooving and associated hole formation is visible along the length of the stripe with a slight increase in hole size and density as the anode is approached. The general features of this roughened Na-doped Au surface are identical to the anode regions of the Li-doped Au samples portrayed in Figures 9, 10 and 11. The uniform grooving is particular to this sample when compared to the largely asymmetrical EM behavior seen previously in the Na-doped films, however, this does illustrate the competitive nature of grain boundary grooving during resistive heating which could be enhanced by alkali out-diffusion. This grooving/alkali out-diffusion dominance in this particular sample is not expected to be related to an unusual structure, as the films described in Figures 14 and 15 were produced under identical deposition conditions. That this sample was stressed at the lowest current density for the Na-doped samples presented here may indicate the importance of test conditions in promoting certain failure mechanisms (See appendix).

The results for K-doped Au thin films are depicted in Figures 16 and 17. The SEM micrographs for the sample in Figure 16, removed prior to failure, give evidence of a very clean surface. Grain delineation

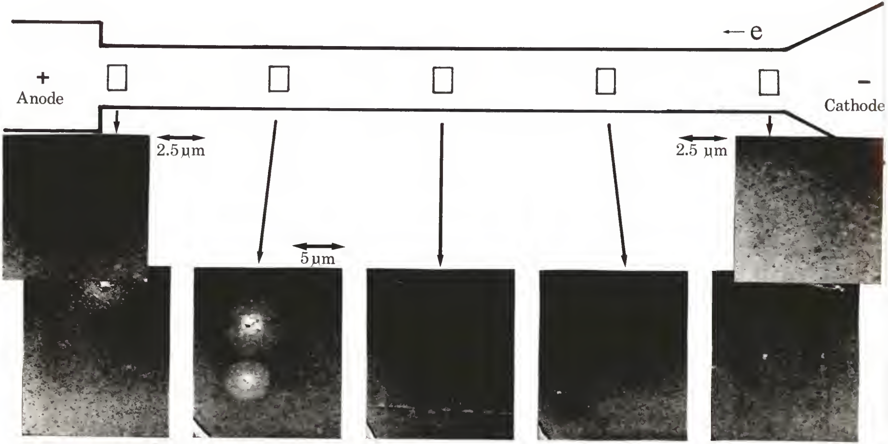

Figure 16. Electromigration Damage Along 800 Å Gold Thin Film Surface (Potassium Borosilicate Substrate).

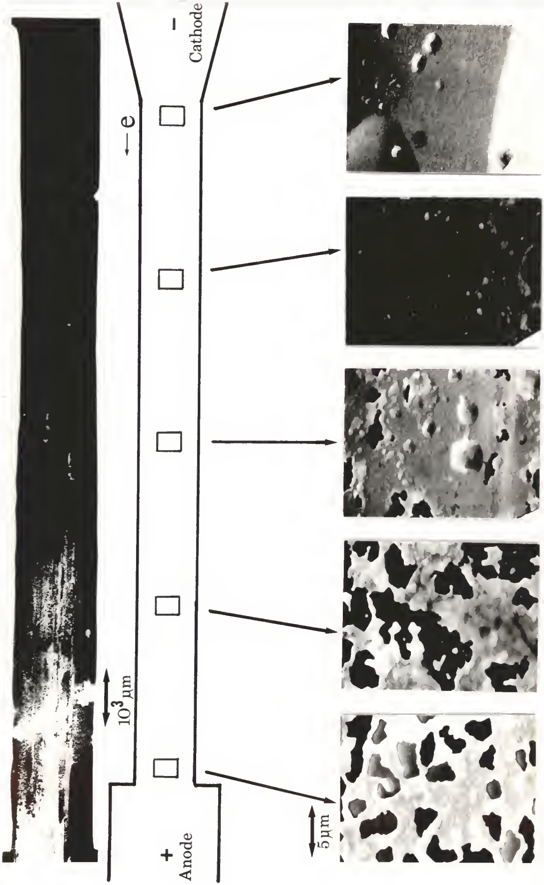

Figure 17. Electromigration Failure of 800 Å Gold Thin Film (Potassium Borosilicate Substrate).

due to grooving is nonexistent. Along the stripe are small pinholes. While the pinhole size remains moderately constant (0.10-0.15 μm), the pinhole density increases from low at the cathode to high at the anode. Although this indicates that the effect due to alkali migration has some importance, the film shows little alkali-induced grooving and hole formation when compared to the effects of the previous Group IA additions. Also, grain boundary grooving and hole formation due to Au depletion at the cathode is not evident.

Failure near the anode is clearly seen in the K-doped Au film presented in Figure 17. While some surface roughening is visible as the cathode is approached, the failure due to the connection of a high density of holes is observed at the anode. These through-holes bear an appearance to those formed by isothermal annealing of Au on K-borosilicate ribbon at 350°C/5 hr and 500°C/5 hr (Figure 6). Some hole formation associated with areas of de-adhesion are seen in the center of the film, similar to the Na-doped Au film in Figure 14.

5.3 Compositional Analysis Using Auger Electron Spectroscopy (AES)

5.3.1 General Description of AES

The determination of the composition of material surfaces using Auger Electron Spectroscopy (AES) is based upon the realization that an atom's electrons are held to its nucleus by precise binding energies. These energies vary from element to element since the size and density of a particular electron cloud configuration varies with Z, the atomic number.

As a material surface is bombarded with energetic electrons, a proportion of these electrons penetrate the electron clouds of the surface atoms, and in some cases dislodge inner electrons. To reduce the energy of these ionized atoms, outer electrons fill the vacancies left by the ejected electrons, generating one of two products. First, energy can be dissipated by the release of an x-ray. Second, the outer electron, while filling the inner vacancy, can impart its excess energy directly to a lower energy electron, causing this Auger electron to be ejected from the atom. The number of x-rays or Auger electrons produced is indicative of the composition of the material surface.

As Figure 18[58] indicates, the Auger yield is near unity (and the corresponding x-ray yield is near zero) for the light elements and remains near unity for L transitions for elements possessing $Z \leq 35$ (and for M transitions for elements possessing $20 \leq Z \leq 35$). Auger production is more efficient than x-ray production within this range since Auger electron wave overlap is more complete for smaller electron cloud distances, and is therefore well suited to tracking the alkali metals.

The basic components of AES are typified by the apparatus used in this work. A beam of 2-5 keV electrons is accelerated towards a clean sample surface. To prevent atmospheric particles from deflecting the incoming electron beam, deflecting the outgoing electrons or chemically interacting with the sample surface, the Auger analysis chamber is held at a vacuum of 10^{-10}-10^{-7} Torr. The Auger electrons are separated by energy as they are collected by a cylindrical mirror analyzer. These electrons possess energies from 20 to 2200 eV and, while a large portion of the signal comes from a surface layer 1-10 Å in depth,[59] 95% of the Auger signal comes from a depth of no greater than approximately 50 Å.[60]

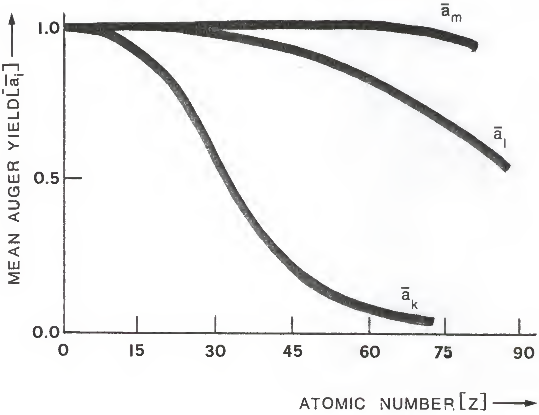

Figure 18. Atomic Number Dependence of the Mean Auger Yield {reproduced by permission from N. C. MacDonald, "Scanning Electron Microscopy/1971," IITRI, Chicago, Illinois (1971), 91.}

It is expected that for a 3 keV electron beam at 50 μAmps, a general Auger detection limit of 0.02-0.20 at.% is attainable when a cylindrical mirror analyzer is used in conjunction with a scanning rate of 1 eV/s.[61]

Two methods of data display currently exist; either the number of electrons detected at a specific energy, N(E) versus E, or the differentiated signal of the same, dN(E)/dE versus E. The differentiation occurs through the use of an additional ac signal applied to the detector. This latter technique was used throughout this work. While the former method of data display allows for the observation of peak shifts and lineshape changes indicative of localized chemical changes along the surface, the latter offers compositional information without the need for background subtraction and deconvolution corrections.

When AES analysis is applied specifically to thin films, two types of physical data acquisition are available. The choice of either the surface accumulation method or the depth profiling technique depends primarily upon the type of diffusion mechanism involved.

The surface accumulation method, in which the Auger signal is collected along the surface of the film, was used throughout this study. M. Wuttig and H. K. Berenbaum in 1966 were the first researchers to use this approach[62] to study coupled grain boundary and dislocation diffusion processes in Ni at low temperatures. The use of this AES technique requires that the diffusant source is located at the substrate/film interface, that the diffusant migrates along the film's grain boundaries, and finally that it collects along the film's surface where it is not restricted by surface diffusion. This technique is applicable to systems where grain boundary diffusion predominates and where boundary volumes are sufficiently small that the amount of diffusant in the overall volume probed by the electron beam represents an amount near or below the AES detection limit. The technique's major drawback is that for samples stressed in environments other than a dedicated AES chamber, a major portion of the recorded Auger signal will be due to surface contamination.

Depth profiling, in which the sample's interior is repeatedly probed after sputtering to remove outer layers, was found to be inadequate for the work reported here. This technique requires leakage of the grain boundary diffusant into the nearby bulk for adequate signal. Since potassium (chosen from the alkali elements for reasons presented below) is not soluble in Au in the solid state,[63] a lattice diffusion mechanism that is competitive with grain boundary diffusion is not anticipated. For the idealized case in which there is complete K saturation of all the grain boundaries in a gold film having a mean grain diameter of 2000 Å, the amount of K would be approximately 0.34 at.%.[64] Since complete packing along every boundary is unlikely and a competitive bulk diffusion mechanism for K in Au does not exist, the amount of potassium contained in the Au films examined here is well below the AES detection limit using the depth profiling technique.

5.3.2 AES Experimental Results and Analysis

Gold films deposited on potassium borosilicate ribbons were chosen for AES analysis, because for the alkali elements studied here, AES sensitivity is the strongest for potassium (See Table 3). Potassium is also least susceptible to electron beam-induced desorption/migration when compared to Li and Na.[48] Such effects reduce the observed alkali

Table 3. AES Parameters For Selected Elements

Material	Atomic Number	Auger Peak Transition	Expected Transition Energy (eV) [a]	Relative Sensitivity [b]
Li	3	KLL (KVV)	43	NA
B	5	KLL (KVV)	179	.149
C	6	KLL (KVV)	272	.170
N	7	KLL (KVV)	381	.325
O	8	KLL (KVV)	503	.500
Na	11	KLL	990	.210
Si	14	KLL	1619	.024
Si	14	LMM (LVV)	92	.340
S	16	LMM (LVV)	152	.770
K	19	LMM (LVV)	252	.790
Au	79	NOO (NVV)	69	.255[c]
Au	79	NNO (NNV)	239	.037[c]
Au	79	NNO (NNV)	255	.021[c]
Au	79	MNN	2024	.018

a) L. E. Davis, N. C. MacDonald, P. W. Palmberg, G. E. Raich and R. E. Weber, Handbook of Auger Electron Spectroscopy, 2nd Ed., Phys. Elec. Div., Perkin-Elmer Corp., Eden Prairie, Minnesota (1976), 19-230.

b) Ibid., 13.

c) Extrapolated from experimental Au Auger reference spectra.

content as the time the electron beam spends on the sample increases, and thereby restricts statistical analysis of the signal. As Table 3 indicates, strong peaks for K, Au, the substrate constituents and common contaminants occur within the energy range of approximately 0-525 eV. By choosing K (252 eV), repeated scanning of this lower energy range allowed for observation of the statistical variation of the primary peaks of interest while minimizing the effects of alkali desorption/migration, hydrocarbon cracking and specimen charging associated with long scanning times.

The Au films analyzed by AES were produced and isothermally annealed or dc stressed in a manner identical to that described in Sections 3, 4.3 and 5.1. In order to restrict the K signal to potassium on the gold surface only, samples were removed from current stressing prior to hole formation. SEM analysis of a representative sample showed no holes at 5400X, where holes with diameters of less than 500 Å are discernible. Also, none of the Auger spectra collected included the major peaks for B (179 eV), Si (1619 eV) or Si in SiO_2 (1606 eV).

After current powering, the K-doped Au samples were immediately placed in the AES vacuum chamber and remained there until the appropriate pressure of 2-90 x 10^{-9} Torr was attained. Data collection consisted of repeated scans within the range of 0-525 eV. Full energy scans (0-2100 eV) were randomly taken several times along each sample adjacent to the areas of interest to insure that no unforeseen contamination had collected along the film surface.

Typical working parameters included V_{acc} = 2 keV, 40 μAmps $\leq I_{beam} \leq$ 100 μAmps, V_{PtP} = 3 eV, τ_c = 100ms (approximately 5-10 eV/s), 1300 $\leq$ multiplier $\leq$ 1500 and a 100 μm beam diameter. An accelerating voltage of 2 keV permitted enhancement of the potassium signal when compared to higher voltages.

The compositional variation was monitored through AES examination of 5 to 8 regions across the length of the sample stripe. Scans of these regions were repeated from 3 to 29 times. Table 3 contains a listing of the primary peak transitions for the elements detected, their expected energies and the sensitivities used. Examples of the original Auger spectra that were collected are displayed in Figure 19. The primary peak energies and peak-to-peak heights are labeled in this figure. The spectra in Figure 19 illustrate the variation in potassium for several sample regions. The potassium LMM transition at 252 eV is noted for an area adjacent to the anode of an EM-stressed Au film on K-borosilicate (Figure 19a), the area adjacent to the cathode of the same EM-stressed Au film (Figure 19b) and a region on an as-deposited Au film on K-borosilicate (Figure 19c). The spectra represent potassium fluctuations of 0% to 15-20% of the total Auger signal for the top few monolayers of film surface.

The variation of potassium along thin Au films as a function of dc stressing is depicted in Figures 20 through 23. In order to semi-quantitatively measure the concentration of K along the stripe surface, the peak-to-peak height of each major transition appearing in the Auger spectrum was measured. These peak height values were inserted into

$$\frac{i(x)/j(x)}{i_{max}/j_{max}} = \frac{PH_i}{PH_j} \cdot \frac{PH_{j,max}}{PH_{i,max}} \qquad (26)$$

where $i(x)/j(x)$ is the ratio of element i to element j at position x, PH_i is the peak height of element i and $PH_{i,max}$ is the maximum peak

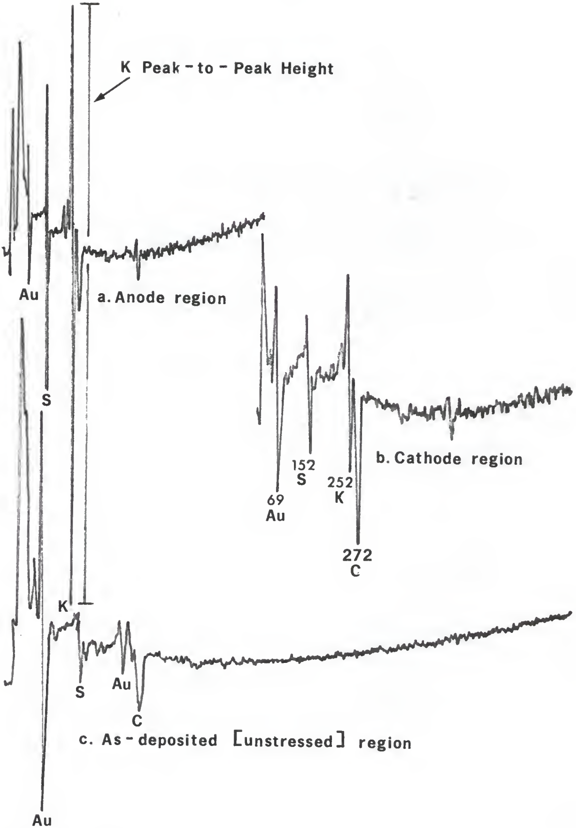

Figure 19. Examples of Auger Spectra from Gold Thin Film Surfaces that Contain Various Amounts of Potassium.

height value for element i measured along the sample. The AES results are displayed as normalized ratios of K/Au, K/S and Au/S that were calculated using equation (26). The areas of AES examination along the stripe are located in a schematic diagram directly above the peak height ratio for that area. Individual film characteristics and test conditions for the Au films discussed here are listed in Table 4.

The portrayal of composition in this form is maintained for several reasons. Since a pure thin film of potassium is thermodynamically impossible to fabricate, the most accurate AES determination of composition using pure standards is impractical. In addition, if such standards could be produced, P. H. Holloway[65] has suggested that at best the composition of a homogeneous binary alloy can be determined confidently only to within 15%. Since the samples examined here are not homogeneous, an accuracy of this sort is not possible. The quantitative analysis is further complicated in that in order to prohibit electron beam effects, it was necessary to use the valence transition for Au at 69 eV. As Table 3 indicates, the Au peaks at 239 eV and 255 eV are valence transitions as well. This makes quantitative analysis using the differentiated Auger signal inappropriate, since, as F. Pons et al.[66] have observed, the differentiated signal can only be studied quantitatively if the primary peaks measured involve core electrons. It is possible, however, to examine the distribution of K along the Au surface qualitatively if such complexities are acknowledged.

In Figure 20, the compositional variation along the surface of an 800 Å Au film deposited on K-borosilicate is depicted. The sample was stored at 25°C (room temperature) for 30 days. No discernible potassium was observed using AES anywhere along the length of the stripe.

Table 4.
Physical Characteristics and Test Conditions for
Gold Films Used in AES Study of Electromigration

Sample Number	GAuK117B	GAuK117C	GAuK118E	GAuK116C
Figure (In Text)	20	21	22	23
Thickness (Å)	810	810	810	500
Initial Deposition Pressure (10^{-8} Torr)	8.5	8.5	4.0	2.1
Deposition Rate (Å/s)	4.2	4.2	6.6	2.7
Initial Resistance (Ω)	---	5.48	5.75	8.20
Final Resistance (Ω)	---	5.10	5.55	7.70
$\bar{J}$ (10^5 Amps/cm^2)	---	8.15	7.08	9.17
Length of Run (hr)	---	552	670	606

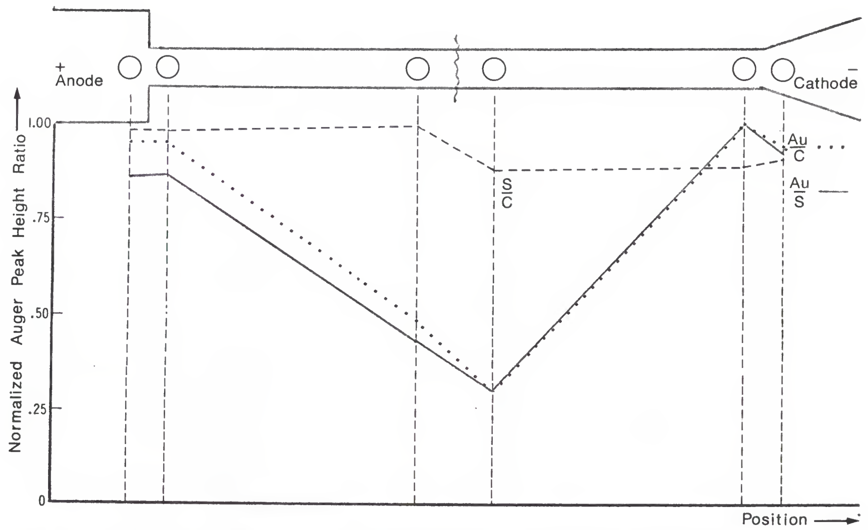

Figure 20. Variation in Normalized Auger Peak Height Ratios as a Function of Position Along the Surface of an As-Deposited Gold Thin Film (Potassium Borosilicate Substrate). (No potassium signal was observed along the length of the film.)

Carbon and sulfur are expected to appear on the sample surface since the sample was exposed to the atmosphere after deposition prior to storage in a covered petri dish. In Figure 20, the amount of Au at either end of the sample is observed to remain fairly constant with a large drop in the Au signal at both points examined in the center of the as-deposited film. This behavior is observed whether the Au signal is referenced to carbon or sulfur. Since the S/C ratio remains quite constant along the stripe, this drop in Au signal must be attributed to contamination. The Auger spectra for these two central regions did differ from the rest of the analyzed areas in this sample in that the oxygen peak at 503 eV was measured only in these two areas. P. Légaré et al. have noted[67] that oxygen on the surface of (111) Au and polycrystalline Au strongly attenuates the 69 eV peak. Such attenuation occurred in this study for both the 69 eV (Au) and 239 eV (Au) peaks.

In Figure 21, the concentration profiles for a K-doped Au film dc-stressed at 8.15 x 10^5 Amps/cm^2 for 552.23 hours are shown. The sharp increase in the K/Au and K/S curves toward the center of the film indicates the role Joule heating plays in accelerating impurity diffusion in the central portion of the powered stripe where the temperature is a maximum. Compositional analysis, based upon the ratio of the sensitivity-corrected K peak height average to the summation of all major peak height averages that have been similarly corrected for Auger sensitivity, shows a threefold increase in K in this area when compared to either electrode region and that the K signal in the center represents approximately one-third of the total AES signal. The sharp rise in the Au/S peak height ratio toward the electrode areas is the result of a large decrease in sulfur contamination. This is caused by experimental procedure in

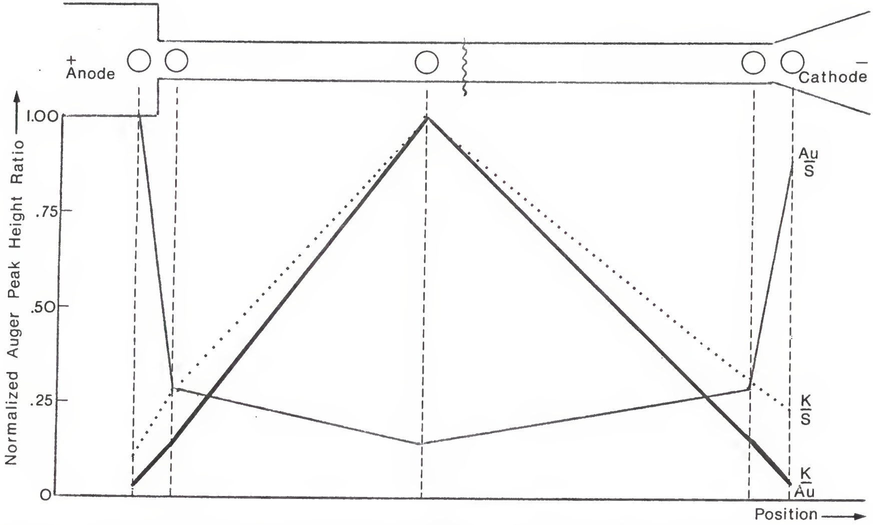

Figure 21. Variation in Normalized Auger Peak Height Ratios as a Function of Position Along the Surface of a Current-Stressed Gold Thin Film (Potassium Borosilicate Substrate).

which the extreme electrode areas are in contact with metal connectors to complete the electromigration circuit. This contact prevents sulfur accumulation in these regions during stressing. The S/C curve for this sample and for those to follow behaved in a manner similar to the as-deposited sample (Figure 20) except for sharp decreases at the extreme electrode regions and is, therefore, not shown. The oxygen content remained relatively constant across the sample, except for no oxygen trace in the extreme anode region where the maximum Au signal was recorded.

In Figure 22 the variation of K content is shown for an 810 Å Au film that was current powered at 7.08 x 10^5 Amps/cm^2 for 669.67 hours. Examination of the normalized K/Au ratio curve indicates that the K concentration is skewed towards the anode. This K build-up at the positive electrode is seen to concur with observations[39,68] that material accumulation in Au during EM is primarily controlled by the electron wind. The high K/Au value at the center of the stripe verifies that K out-diffusion due to Joule heating remains a competitive mechanism in spite of the electron wind-induced drift of potassium. Compositional analysis indicates that the K concentration for the film surface represents approximately 30% of the total Auger signal in the central region, nearly 40% at the positive terminal and 15-20% at the negative terminal. The Au/S curve is reduced near the anode due to K coverage and rises near the cathode. The K/S curve is rather constant until a drop at the cathode. This reduction occurs due to decreased K rather than increased S since the Au/S curve for the same region rises sharply. The oxygen content remained low and constant across the entire film.

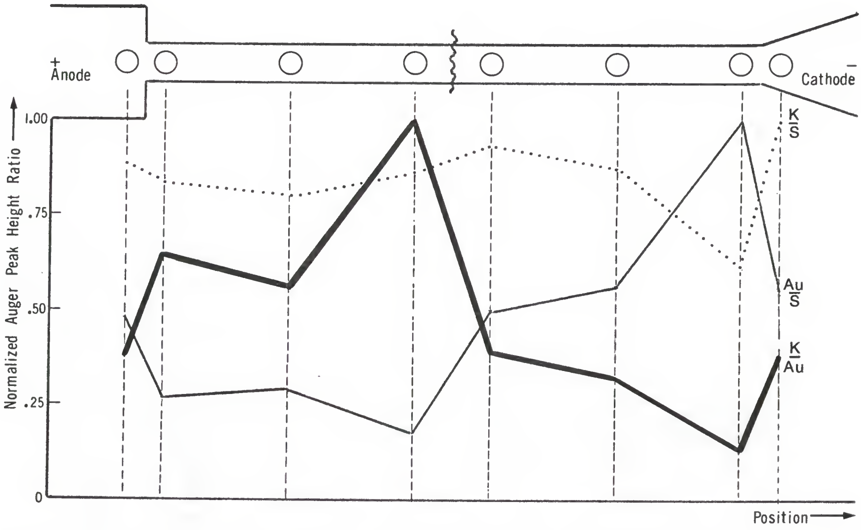

Figure 22. Variation in Normalized Auger Peak Height Ratios as a Function of Position Along the Surface of a Current-Stressed Gold Thin Film (Potassium Borosilicate Substrate).

Finally, in Figure 23 another example of EM-induced migration of K is shown. This 500 Å K-doped Au film was stressed for 605.81 hours at 9.17 x 10^5 Amps/cm^2. The behavior of both the K/Au and K/S curves are identical to those of the previous sample in exhibiting K build-up at the anode due to the electron-solute interaction. The Au/S curve, in contrast to the previous sample, does not exhibit low Au signal in regions of high K signal and vice versa. Rather, the Au/S curve remains high at both electrodes with a depression at the center. While the reason for this behavior is unclear it does authenticate the asymmetrical behavior of the K signal. The variation in K signal across the surface of the stripe ranges from 13% of the total signal at the center to 7% at the anode and 1-2% at the cathode. While the asymmetry of potassium appears more extreme in this sample compared to the previous film, this is due in part to the high level of contamination seen in this particular sample, where the combined carbon and sulfur peaks represent 60-75% of the total AES signal. K out-diffusion is still competitive with the electromigration process.

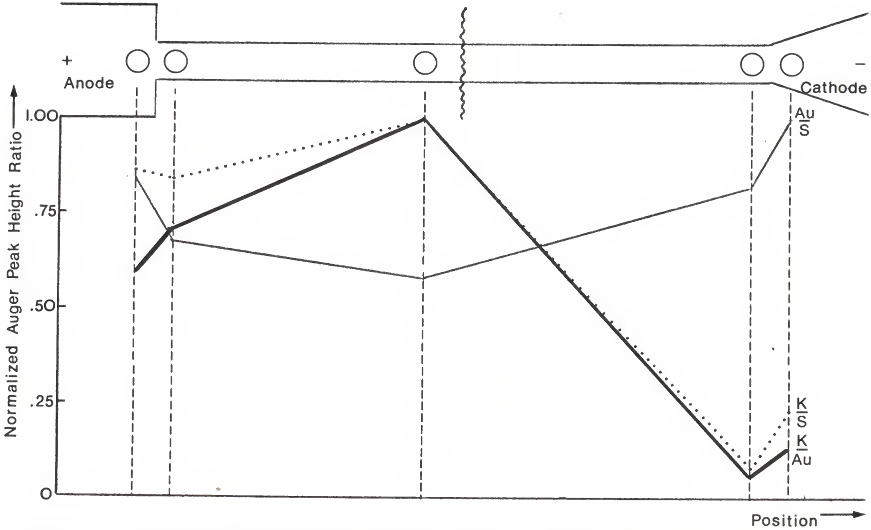

Figure 23. Variation in Normalized Auger Peak Height Ratios as a Function of Position Along the Surface of a Current-Stressed Au Thin Film (Potassium Borosilicate Substrate).

CHAPTER 6
REACTIVE NATURE OF THE ALKALI ELEMENTS

6.1 Introduction

It was implied earlier (Sections 4.3, 5.2 and 5.3.2) that the Group IA elements rapidly reached the surface of 800 Å Au thin films during isothermal heat treatment or during dc stressing. This was appreciated by the examination of SEM micrographs and AES profiles of said films after both testing regimes. While pure Au films deposited on quartz were resistant to heating at temperatures up to 560°C/1 hr, similar films deposited on alkali borosilicate ribbons were observed to degrade severely after an anneal of 350°C/5 hr. Hole formation was so severe in Au films deposited on Na-borosilicate substrates that these films barely maintained continuity after a heat treatment of 500°C/5 hr in air. (Film degradation was more severe for Au films deposited on Na-microscope glasses that were annealed at 560°C/1 hr in 1 Torr air.) Damage modes in these doped films included grooving along grain edges in contact with the environment, the formation of holes that penetrate the films' thicknesses, grain sliding adjacent to these holes and the accumulation of non-conducting surface material.

After dc stressing, alkali-doped Au films again exhibited structural changes far different from their pure Au counterparts. The general appearance of the alkali-contaminated film surfaces was observed to be far more roughened than the film surfaces of pure Au. Alkali-doped Au films were also seen to degrade more rapidly than similarly tested pure

Au films. In addition, failure of the alkali-doped Au films was more difficult to describe in that the electromigration-induced hole coalescence leading to failure was not restricted to the cathode portion of the stripe as was the case for pure Au films. In fact, failure occurred at either end of the alkali-doped stripes. The surface degradation of Na-doped and K-doped Au films due to alkali accumulation at the anode closely paralleled that of similar film surfaces that were subjected to the higher temperatures (350°C/5 hr and 500°C/5 hr) of the above-mentioned heat treatment. AES analysis of K-doped Au films that were dc stressed and removed prior to the formation of holes indicated that proceeding hole formation at the anode a high concentration of potassium collects in that region. The maximum amount of K was found at the center of the stripe where the maximum temperature during testing occurs.

Because the anode during dc stressing was not heated to the higher annealing temperatures, it is postulated that the similarities in the anode areas of the dc stressed samples with the surfaces of heat treated samples were produced by an increased concentration of alkali impurity when compared with that of the annealed samples. This increased concentration is the result of the electron wind-solute interaction. It is finally proposed that the failure location depends upon whether alkali accumulation at the anode, followed by grain boundary grooving, proceeds at a faster rate than Au depletion at the cathode. The location would vary as a function of impurity levels, current density and the environment during testing.

Such a model requires rapid alkali out-diffusion through the Au film and it is necessary to examine mechanisms for alkali disassociation from the glass and for alkali transfer through the Au film. It is postulated that by entering the Au film, the alkali elements respond to the chemical potential gradient that exists through the thickness of the films, thereby lowering the energy of the system with respect to the solute. Simultaneously, by entering the Au film, the alkali impurities reduce the surface and grain boundary energies of the Au film by adsorption, thereby lowering the energy of the system with respect to the solvent. Reduction of the vertical gradient never occurs, however, because once the alkali reaches the Au surface, oxidation removes the species from the diffusion process keeping the rate of alkali transfer high.

Alkali adsorption and oxidation are independent of and superimposed upon the electrical potential gradient and generally increased rates of diffusion caused by the application of an electric field and associated Joule heating. That hole formation doesn't necessarily require mass depletion, but rather mass readjustment, will be discussed.

6.2 High Alkali Mobility in Glassy Structures

The basic structural units of a silica glass matrix are interconnected tetrahedra. In these glasses, the tetrahedra consist of a central, highly charged positive Si ion surrounded by four oxygen ions. To preserve electrical neutrality, each of these oxygen ions are then bonded to four more Si ions, producing a chain of SiO_2 molecules. The high +4 charge of the Si ion promotes stability in the glass because all of the oxygen ions are bonded. Boron, another highly charged cation, behaves similar to Si in producing chain stability. Its lower charge of +3, however, allows for alkali additions because these cations of +1 charge provide electrical neutrality. T. Furukawa and W. B. White[69] have shown that for borosilicate glasses having $Na_2O/B_2O_3 < 1$, (the glasses used in this work contained $Na_2O/B_2O_3 \approx 0.375$), all of the network-modifying cations are associated with borate groups. This configuration maintains electrical neutrality at the cost of glass stability, since oxygen ions can now partially bond to the Na cations outside of the chain, which breaks up the glass network.

This network break up combined with the comparatively small radii and electrical charge of the alkali elements, makes the alkali constituents the only mobile species in the glass. Their mobility is also relatively high.[70] The open, random structure of the glass offers large interstices for alkali diffusion. In addition, since the alkali ions are not integral members of the structure, little energy need be supplied to break their bonds to induce movement. The high mobility of these cations is further enhanced at increased alkali concentrations, since additional Na^+'s break up more Si-O bonds, opening the structure further.

The high mobility of the alkali elements can be appreciated by an examination of their oxide bond strengths and radii when compared to Si and B. As Table 5 indicates, the bond strengths for the network-modifying alkalies with oxygen are one-third to two-fifths the values of those associated with Si and B, making the alkali oxides more susceptible to disassociation at moderate temperatures. Within the alkali group, as the atomic number and ionic radius increase, the oxide bond strength decreases. Competition between these two parameters is responsible for the experimental observation that of the alkalies in high purity SiO_2 glass, the Na^+ ion is the most mobile (See Table 5). The high oxide bond strengths of Si and B prohibit measurable movement.

Measured values for alkali diffusion in various glasses exist in great quantity in the literature. These values vary extensively because

Table 5. Bonding Characteristics of Glass Constituents

Element	Atomic Number	Valence	Oxide Bond Strength (kcal/mole) a)	Radius (Å) b)	Relative Mobility c)
Li	3	+1	Li-O: 84.1 ± 1.5	0.68	0.15
Na	11	+1	Na-O: 61.3 ± 4.0	0.97	1
K	19	+1	K-O: 57 ± 8	1.33	< 0.002
B	5	+3	B-O: 192.7 ± 1.2	0.23	
Si	14	+4	Si-O: 190.9 ± 2.0	0.42	
Cr	24	+3	Cr-O: 102 ± 7	0.63	
Ag	47	+1		1.26	0.08
Au	79	+1		1.37	

a) Oxide bond strength determined at 298°K from R. C. Weast, ed., Handbook of Chemistry and Physics, 57th edition, CRC Press, Cleveland, Ohio (1976), F219-F225.

b) Ibid., F-213.

c) Relative mobility was measured at 653°K in SiO_2 glass prepared from natural quartz crystals by R. H. Doremus, Phys. Chem. Glasses, 10 (1969), 28-33.

glass processing, minute levels of contamination and water content have a strong effect upon measured diffusion parameters and have, until recently, often gone unreported. For a typical silica glass that contains 30.0-33.3 mole% $(IA)_2O$ and for the temperature range of 300-500°C, a broad estimate for the diffusion parameter for Na[71] and K[71] is $D_0 \cong 1\text{-}2 \times 10^{-3}$ cm^2/s with the activation energy for Li,[72] Na[71] and K[71] diffusion approximated at 16 kcal/mole. While these alkali contents are greater than those used in the work reported here, because the latter contained B_2O_3 the anticipated diffusion coefficients should be comparable. When the above activation energy value is compared to that of Cr grain boundary diffusion in Au at comparable temperatures ($Q_{gb}^{Cr\ in\ Au}$ = 26 kcal/mole[73]), the alkali mobility in glass is seen as high.

In order to understand how the alkali elements enter the Au film during heating and dc stressing, it proves helpful to examine the alkali glass surface without any coating or film. It has been repeatedly shown that for Na glasses the activity of Na within the glass is very sensitive to the ambient[74] and that in air, the outermost surface of a Na glass is rich in Na and Na compounds, with the underlying region of the glass being depleted in Na. This surface enrichment aids in surface energy reduction, for the out-diffusion of Na acts specifically to annihilate surface defects along the silicate glass surface.[75] This 'dealkalization' process can be enhanced by increased temperatures or by the application of an electric field.[76] G. Keppeler and M. Hechter[77] found for a glass containing 18.5% Na_2O, that the surface concentration of alkali oxide continually increased with time, for a maximum of seven hours, for annealing temperatures of 450 to 550°C. Only after an anneal at 575°C did the Na_2O amount on the surface decrease due to evaporation.

In another study,[78] 20.0% of the Li_2O in a silicate glass and 39.3% of the K_2O in a similar glass migrated to the surface of each glass upon heating to 550°C in a SO_2-O_2 atmosphere to collect at the surface as alkali sulfates. Recently, C. G. Pantano et al.[79] have shown for a glass containing both Na and Ca, that a several minute exposure to a small amount of air in an AES UHV chamber produces a 50 Å deep surface layer of Na_2O and CaO contamination while depleting up to the first 800 Å of the glass of Na and Ca. Since such surface layers are appreciably thicker than the one monolayer needed to annihilate glass surface defects,[47] film growth beyond one monolayer persists to reduce the free energy of the alkali species through oxidation (See Section 6.3). L. L. Hench[80] has noted that for glasses containing equivalent mole% of alkali oxide, the rate of attack increases with alkali atomic number. It is expected, then, that the outermost surface of all alkali borosilicate glasses used in this work consisted of an alkali-rich contamination layer.

When submerged in liquids, alkali silicate glasses leach out the Group IA elements, causing the glass surface to be deficient in alkali oxide.[81]

The above examples illustrate that not only are the alkali ions highly mobile in the glass of which they are a part, but that they routinely collect on or near the glass surface. For Au films deposited on alkali glasses, this increased alkali surface concentration enhances the already poor adhesion between Au and glass.[82] Since Au does not readily oxidize at moderate temperatures, in contrast to most metals, chemical bonding does not occur at the Au/glass interface. It has been shown that as a metal's free energy of oxide formation becomes more negative, adhesion between a metallic species and the glass improves.[83]

This lack of adhesion between Au and the substrate gives rise to an extremely disorganized Au/substrate interface which facilitates movement of any species that collects there.

If it is assumed that the alkali elements easily collect at the film/substrate interface and that they reduce the interfacial energy there, it still must be determined why these impurities then enter the Au film rather than remain at the interface. The catalytic effects of potential gradient reduction and subsequent oxidation of the solute with the simultaneous reduction of the solvent's various surface energies by alkali out-diffusion provides a possible mechanism.

6.3 Free Energy of Alkali Oxide Formation

The high surface-to-volume ratio of thin films accentuates the effect of the film/environment interface on the film's behavior during testing. G. C. Nelson and P. H. Holloway[73] verified, using AES and SIMS, that Cr from an intermetallic adhesive layer reached the surface of a 3400 Å Au film after short times when the sample was heated at 211 to 293°C in an oxidizing atmosphere. The amount of Cr and O_2 that collected along the surface increased with the time length of the diffusion anneal. Little Cr was found on samples heated in vacuum. The researchers concluded that this Cr out-diffusion was driven initially by the solute potential gradient but maintained by the negative heat of Cr_2O_3 formation.

C. A. Chang[34] found that the Au film/environment interface can either enhance or reduce solute diffusion through 2000-3000 Å Au films. Both Si (from a Si(111) substrate) and Cr (from a 2000 Å adhesion layer) were observed to collect faster along the surface of the film as the oxidizing nature of the ambient increased. The diffusion of Cr and Si through Au films could be suppressed by introducing CO into the environment. The same occurs for Co, Cu,Ga and As out-diffusion through Au thin films. The researcher describes this effect based upon the relative charge or 'ionicity' of the solute with respect to the solvent and the effect of atmospheric adsorption in altering the work function of the films' grain boundaries and outside surfaces. When the solute is positive relative to the matrix and the ambient reduces the work function of the matrix, out-diffusion of the solute is improved.[34]

Both G. C. Nelson and P. H. Holloway[73] and C. A. Chang[34] experimentally observe increased Cr concentration along a Au thin film in spite of differing approaches.

Calculated values for the standard Gibbs free energy of formation, ΔG^o, for a variety of oxides and compounds are listed in Table 6. All reactions listed were normalized for 1 mole of the reactive gas. The majority of reactions listed were chosen to depict possible alkali products relevant to the annealing and dc stressing results presented in this work, with temperatures chosen to correlate with those used in the annealing study. Several additional reactions are listed for comparative purposes. In many instances, other possible oxide and compound forms exist. These are not presented here since the tabulated free energies of formation for these unlisted forms indicate that they are not thermodynamically favored when compared to those listed in Table 6.

An examination of the calculated ΔG^o value for Cr_2O_3 formation confirms the analysis put forth by C. G. Nelson and P. H. Holloway[73] that Cr out-diffusion is maintained in oxidizing environments because of the formation of Cr_2O_3. Free energy values of -168,760 to -148,743 cal/mole O_2 for the temperature range of 25 to 500°C are indicative of

Table 6. Standard Gibbs Free Energy of Formation, ΔG^o
(Normalized for 1 Mole Reactive Gas)

Reaction	Standard Free Energy of Formation, ΔG^o			
	25°C	200°C	350°C	500°C
*C(graphite) + $O_2(g) = CO_2(g)$	-94,252	-94,360	-94,430	-94,482
*$1/2S_2(g) + O_2(g) = SO_2(g)$	-81,310	-78,291	-75,664	-73,024
*$2Li(c) + O_2(g) = Li_2O_2(c)$	-136,550	-127,620a)	---	---
*$4Li(c) + O_2(g) = 2Li_2O(c)$	-267,608	-257,156a)	-246,978	-236,504
**$2/3Li_2O(c) + 2/3CO_2(g) = 2/3Li_2CO_3(c)$	-26,789	-23,320	-16,597	-11,950
*$2Na(c) + O_2(g) = Na_2O_2(c)$	-107,050	-97,874a)	-89,920	-82,386b)
*$4Na(c) + O_2(g) = 2Na_2O(c)$	-179,744	-167,860a)	-157,268	-146,746
**$4Na(c) + S_2(g) = 2Na_2S(c)$	-191,952	-182,142a)	-172,482	-163,320
**$2Na(c) + Cl_2(g) = 2NaCl(c)$	-184,034	-176,665a)	-169,495	-163,022
**$2/3Na_2O(c) + 2/3SiO_2(c) = 2/3Na_2SiO_3(c)$	-37,418	-37,577	-37,683	-37,816
**$1/2Na_2O(c) + 1/2SO_3(g) = 1/2Na_2SO_4(c)$	-62,266	-58,905	-56,042	-53,428
**$2/3Na_2O(c) + 2/3CO_2(g) = 2/3Na_2CO_3(c)$	-44,216	-40,581	-37,444	-34,357

Table 6 (continued). Standard Gibbs Free Energy of Formation, ΔG^o
(Normalized for 1 Mole Reactive Gas)

Reaction	Standard Free Energy of Formation, ΔG^o			
	25°C	200°C	350°C	500°C
$^*4/3K(c) + O_2(g) = 2/3K_2O_3(c)$	-68,441	---	---	---
$^*4K(c) + O_2(g) = 2K_2O(c)$	-152,584	-139,768a)	-128,504b)	-117,204
$^*2K(l) + O_2(g) = K_2O_2(c)$	---	-89,325	-78,074	-76,145b)
$^{**}2K(c) + Cl_2(g) = 2KCl(c)$	-194,591	-186,225a)	-179,254	-172,184
$^{**}2/3K_2O(c) + 2/3CO_2(g) = 2/3K_2CO_3(c)$	-54,971	-50,623	-46,921a)	-43,154
$^*4/3Cr(c) + O_2(g) = 2/3Cr_2O_3(\beta)$	-168,760	-161,262	-154,963	-148,743
$^*Si(c) + O_2(g) = SiO_2(\alpha\text{-quartz})$	-196,913	-189,281	-182,776	-176,345
$^*4/3Au(c) + O_2(g) = 2/3Au_2O_3(c)$	+12,376	+19,829	---	---
$^{**}4Ag(c) + S_2(g) = 2Ag_2S(c)$	-37,843	-34,457c)	-31,967	-29,378

*Values necessary for calculations taken from R. C. Weast, ed., Handbook of Chemistry and Physics, 57th edition, CRC Press, Cleveland, Ohio (1976), D45-D50.

**Values interpolated from T. Rosenqvist, Principles of Extractive Metallurgy, 2nd edition, McGraw-Hill, Inc., New York (1983), 486-497.

a) reactant melts
b) product melts
c) product transforms

a highly exothermic reaction. The formation energies of SiO_2(α-quartz), ranging from -196,913 to -176,345 cal/mole O_2, for the same temperature range, define a slightly more stable oxide. This strong tendency for Cr_2O_3 and SiO_2(α-quartz) production gives credence to C. A. Chang's observations,[34] although from a different analytical perspective. The stability and 'spontaneity' of these two oxides can be appreciated after an examination of the ΔG^o values for the production of CO_2 and SO_2 (See Table 6) in that the ΔG^o values for these latter reactions are approximately one-half the magnitude of the Cr_2O_3 and SiO_2(α-quartz) oxidation reactions for the same temperature range.

The calculated values of the free energy of alkali oxide formation in the same temperature range are comparable to or larger than those listed for Cr_2O_3 and SiO_2(α-quartz). ΔG^o values for Li_2O range from -267,608 to -236,504 cal/mole O_2, ΔG^o values for Na_2O range from -179,744 to -146,746 cal/mole O_2 and ΔG^o values for K_2O range from -152,584 to -117,204 cal/mole O_2. As the alkali atomic number increases, the amount of energy release upon oxidation decreases.

Comparison of the energy of formation of Na_2O with that of the ionic compound NaCl, and to a lesser extent that of K_2O with that of KCl, indicates that these reactions are also somewhat competitive. Na_2O formation is also competitive with sodium sulfide production.

These rudimentary calculations indicate, as well, that unless some unforeseen mechanism exists, the production of alkali carbonates and silicates would not be favored over oxide production. For example, the free energy of disodium silicate formation, ranging from -37,418 to -37,816 cal/mole O_2, is one-fifth to one-fourth that of Na_2O production. This comparison gives a general indication of the weak bonding of the alkali elements to the glass matrix, and hence, an indication of the higher initial activity of the alkali elements in the glass compared to their activity in the final oxide.

The energy of Au_2O_3 formation is small and positive which demonstrates that Au is relatively inert in oxidizing atmospheres.

It has been shown that the calculated values for the free energy of Li_2O, Na_2O and K_2O formation are very large and negative, and that these values are comparable to those calculated for Cr_2O_3 and SiO_2(α-quartz) formation. The stability of these alkali oxides becomes increasingly apparent after examination of the calculated values of the free energy associated with CO_2 and SO_2 production. At all of the temperatures considered, the magnitude of the free energy of formation of the alkali oxides, Cr_2O_3 and SiO_2(α-quartz) indicate that these oxides are substantially more stable than either CO_2 or SO_2. Considering these calculations, the results of other investigators[34,73] and the SEM and AES results presented earlier, it is believed that the oxidation of the alkali impurities indirectly aids in the mass transfer of the alkali elements from the glass, through the glass/film interface, through the Au film and finally to the film's surface.

In situations where solute diffusion is unaffected by the environment, alkali migration would begin in response to a large potential gradient that exists through the film thickness at the beginning of the process. The initially large solute concentration gradient would continually decrease as diffusion progressed until the steady state was reached and then maintained. This would be the case for Au films that contain solutes not susceptible to oxidation or for alloyed Au films in reducing atmospheres.

For the alkali solutes, however, the formation of an oxide is thermodynamically required. Once the alkali reaches the film surface (or enters gold grain boundaries onto which oxygen has adsorbed), the oxidation process removes the pure species from the transfer process originally activated by the potential gradient. Since the solute concentration gradient is not reduced, the rate of alkali mass transfer would remain high with continuous accumulation of the solute along the Au surfaces, assuming no orientation restrictions with regard to surface diffusion.

6.4 Size Considerations

The grain boundary width in thin films is typically approximated to be 5-10 Å[84] and it is often anticipated that the ease with which a solute species migrates through the grain boundary decreases as solute radius increases. The ionic radii for the alkali elements increase with atomic number from 0.68 Å for Li to 1.33 Å for K. Li and Na have radii one-half and seven-tenths that of the solvent whereas K and Au possess almost identical radius sizes.

The ionic radii for Cr, Ag and Au are 0.63 Å, 1.26 Å and 1.37 Å respectively (See Table 5). The activation energies for Cr, Ag and Au grain boundary diffusion in Au thin films at temperatures below 300°C are 1.13 eV,[73] 0.62 eV[85] and (0.88 ± 0.06) eV[13] respectively. Clearly these experimentally determined activation energies are not solely related to radius size. Additional solute parameters such as the effective charge, grain boundary bond type and energy, solubility and others make size considerations alone insufficient in determining solute diffusion rates along grain boundaries.

6.5 Surface Energy Reduction

While the initial concentration gradient through the film thickness drives the alkali through the film to its surface, alkali diffusion in response to this gradient alone fails to describe several experimental observations. Enhanced diffusion rates caused by alkali oxidation at or near the film surface do not explain these same observations, which are related to the Au film surface itself. These include the rapid degradation of alkali-doped Au films after annealing, the rapid and severe degradation of Au films where AES analysis indicates higher levels of alkali (potassium) impurity after some dc stressing, and the variation in character of EM failure in alkali-doped Au films as a function of position of failure. In addition, it was seen that for those alkali-doped films that failed in the anode region after dc stressing, the surface of the anode region was similar to that noted in alkali-doped Au films subjected to heat treatments alone as opposed to 'typical' electromigration failure in the same films when Au depletion produced cathode failure. None of the mechanisms discussed thus far offers insight into the behavior of the Au films as affected by alkali impurities.

Since enhanced grain boundary grooving and associated hole formation in metals are the results of surface energy reduction due to increased temperature and/or impurity adsorption along the metals' higher energy surfaces, an understanding of surface energy requirements appears essential.

Grain boundary grooving occurs in most metals subjected to elevated temperatures. Grooves form along grain boundaries that are in contact with the sample's external surface. This external, solid-vapor surface is characterized by a surface energy, σ_{sv}. At low temperatures grooves rarely form because the external surface, which separates two phases that also differ in composition, has a σ_{sv} that is much larger than the grain boundary interfacial energy, γ_{gb}, which describes a surface separating two volumes that differ only by crystallographic mis-match. Grooves form in systems where either an increase in temperature or adsorption along the external surface reduces σ_{sv} faster than γ_{gb}. Under these conditions, the grain boundary interface becomes the high energy surface and its area is reduced[86] to lower the system's overall energy at this new temperature and/or surface composition.

Experimental values of σ_{sv} and γ_{gb} for the materials of interest in this study are listed in Table 7. The rates of change with temperature of σ_{sv} and γ_{gb} are also listed. For the temperature range of 925 to 1000°C, the solid-vapor surface energies for Cu, Ag and Au are 1.780, 1.400 and 1.100 J/m^2 respectively. Grain boundary energies for the same temperature range are 0.625, 0.378 and 0.375 J/m^2 respectively. In the same temperature range the rate of change of σ_{sv} with temperature for these metals is four to five times faster than the same for γ_{gb}. Both the solid-vapor surface energy and the grain boundary interfacial energy for these metals decrease as temperature increases, and the former continues to decrease faster than the latter as the temperature increases.

In metals which groove at elevated temperatures, the grooving occurs because of the relationship between $d\sigma_{sv}/dT$ and $d\gamma_{gb}/dT$ alone or in concert with impurity adsorption along the free surface. The impurities come either from the sample itself or from the atmosphere to segregate along the surface thereby lowering its surface energy rapidly. Impurity adsorption does not always reduce σ_{sv}. Whether an impurity chemi- or physisorbs on the surface, and depending on the size and orientation

Table 7. Experimental Values for Selected Surface Energies

Metal/Alloy	T (°C)	Liquid-Vapor Surface Energy a)	Solid-Vapor Surface Energy b)		Grain Boundary Surface Energy c)	
		γ_{lv} (J/m^2)	σ_{sv} (J/m^2)	$d\sigma_{sv}/dT$ (J/m^2-°C)	γ_{gb} (J/m^2)	$d\gamma_{gb}/dT$ (J/m^2-°C)
Cr	1950>T_m	1.590	--	--	--	--
	1400	--	2.300	--	0.920	--
Cu	1083 (T_m)	1.300	--	--	--	--
	925	--	1.780 (1.580*)	-0.50×10^{-3}	0.625	-0.10×10^{-3}
Au-20 w/o Cu	1300	1.110	--	--	--	--
	850	--	1.140	--	0.320	--
Au-40 w/o Cu	850	--	0.910	--	0.310	--
Au-50 w/o Cu	1300	1.150	--	--	--	--
Au-60 w/o Cu	850	--	0.930	--	0.390	--
Au-80 w/o Cu	1300	1.200	--	--	--	--
	850	--	1.160	--	0.430	--
Au	1063 (T_m)	1.140	--	--	--	--
	1000	--	1.400 (1.400*)	-0.43×10^{-3}	0.378	-0.10×10^{-3}
Au-31 w/o Ag	1108	1.029	--	--	--	--
Au-55 w/o Ag	1108	0.982	--	--	--	--
Au-67 w/o Ag	1108	0.945	--	--	--	--
Au-79 w/o Ag	1108	0.917	--	--	--	--
Ag	1000	0.895	--	--	--	--
	950	--	1.100 (1.100*)	-0.47×10^{-3}	0.375	-0.10×10^{-3}

Table 7 (continued). Experimental Values for Selected Surface Energies

Metal/Alloy	T (^oC)	Liquid-Vapor Surface Energy a) γ_{lv} (J/m^2)	Solid-Vapor Surface Energy b) σ_{sv} (J/m^2)	$d\sigma_{sv}/dT$ (J/m^2-^oC)	Grain Boundary Surface Energy c) γ_{gb} (J/m^2)	$d\gamma_{gb}/dT$ (J/m^2-^oC)
Li	180 (T_m)	0.398	--	--	--	--
Na	98 (T_m)	0.191	--	--	--	--
K	64 (T_m)	0,101	--	--	--	--
Si	1410 (T_m)	0.730	--	--	--	--
NaCl (100)	low	--	0.300 d)	--	--	--

a) L. E. Murr, *Interfacial Phenomena in Metals and Alloys*, Addison-Wesley Publishing Co., Reading, Massachusetts (1975), 101-106.
b) Ibid., 124-125.
c) Ibid., 131-132.
d) R. A. Swalin, *Thermodynamics of Solids*, 2nd edition, John Wiley and Sons, Inc., New York (1972), 234.

*) Values calculated using the method of W. R. Tyson and W. A. Miller, Surf. Sci., 62 (1977) 267-276.

restrictions of the complex so-formed, the predominant transfer mechanism needed to produce the grooves can be enhanced or suppressed.

Through experimental measurement of groove width and height, the coupling of σ_{sv} and γ_{gb} with the dominant mass transfer process at the groove is commonly obtained through the use of equations such as those developed by W. W. Mullins.[87] Since the mass transfer mechanism and the degree of adsorption are usually not well known, most grooving experiments deliver values of the ratio γ_{gb}/σ_{sv} until one of the two surface energies can be determined independently.

The experimental determination of σ_{sv} is difficult and only a small number of σ_{sv} values exist in the literature. The standard method used to extract σ_{sv} is the zero-creep test using a thin foil or fine wire of the metal of interest. Although the methodology of the test is well known, there are two major difficulties inherent to the test. Precise measurement of the load at which zero-creep occurs is difficult and problems associated with conducting high temperature testing arise because the samples must be tested near their melting points to eliminate the dependence of σ_{sv} on crystallographic orientation.

Such difficulties do not exist when the measurement of the liquid-vapor surface energy, γ_{lv}, is pursued and therefore, values of γ_{lv} are well represented in the literature. While surface cleanliness is still crucial, surface tension/energy measurements of the liquid-vapor interface energy employing the sessile drop, pendent drop and drop weight tests offer more tractable data collection. Experimental values for γ_{lv} appear in Table 7.

It is then possible to estimate a value for a metal's σ_{sv} by inserting the value of γ_{lv} so collected in an empirical relation of the form[88]

$$\sigma_{sv}(T) \simeq 1.2\gamma_{lv}(T_m) - 0.45(T_m - T) \tag{27}$$

where T_m is the melting point of the metal and the temperature at which $\gamma_{lv}(T_m)$ is actually measured and T is the temperature of interest. L. E. Murr[88] has indicated that equation (27) is valid for FCC and BCC metals. The solid-vapor surface energy is larger than γ_{lv} as estimated by equation (27) and σ_{sv} increases as temperature decreases. Additional γ_{lv} values for the alkali elements are listed in Table 7 to permit later calculations. That the liquid-vapor surface energies for the alkali elements are 2.5 to over 10 times smaller than most listed in Table 7 should be noted.

W. R. Tyson and W. A. Miller[89] utilize the experimentally measured γ_{lv}'s to determine $\sigma_{sv}(T)$ in a similar manner but based upon several fundamental principles. The researchers develop an equation of the form[89]

$$\sigma_{sv}(T) - \sigma_{sv}(T_m) = \int_T^{T_m} (S_{sv}/A)\, dT \tag{28}$$

where S_{sv} is the surface entropy and is the sum of the surface's vibrational and configurational entropies, A is the surface area associated with one mole of surface atoms and is approximated as[90]

$$A \simeq 1.612\, N^{1/3}\, V^{2/3} \tag{29}$$

and N is Avogadro's number. V is the molar volume of the species in question. Using approximations for S_{sv}, the authors construct a master curve from which values of $\sigma_{sv}(T) - \sigma_{sv}(T_m)$ can be determined as a function of the reduced unit T/T_m.

The values calculated for $\sigma_{sv}(T)$ using the method of W. R. Tyson and W. A. Miller[89] for selected elements for the temperature range of 25 to 500°C are portrayed in Table 8. Also listed are values for the various constants needed to arrive at the $\sigma_{sv}(T)$ values. (As a check, values for $\sigma_{sv}(T)$ for Cu, Ag and Au were calculated using this method for temperatures at which $\sigma_{sv}(T)$ has been experimentally determined. For comparison, these values are listed beside those experimental values in Table 7. Very good agreement between the calculated and experimental $\sigma_{sv}(T)$ values is observed.)

While examining these calculations, several observations can be made. At room temperature, the solid-vapor surface energies of the alkali elements are low compared to those of the noble metals and are 3 to 12 times smaller than σ_{sv} for Au. Within the alkali group, σ_{sv} decreases with atomic number in direct response to the linear dependence of $\sigma_{sv}(T)$ on T_m. At the higher temperatures considered, at which the alkali elements are no longer solid, the every decreasing liquid-vapor surface energies (with increasing temperature) would be even lower than the already low solid-vapor energies calculated for the alkali elements.

At temperatures of 200°C and above, Si always has a lower σ_{sv} while Cr always has a much higher surface energy compared to Au and the other noble metals, again demonstrating the dependence of σ_{sv} on T_m. The order of the solid-vapor surface energies never changes among these metals at any temperature.

These calculations indicate that it is likely that additions of the alkali elements and Si could reduce the solid-vapor surface energy of Au during annealing and dc current stressing in a manner similar to Au additions to copper and Ag additions to gold as depicted in Table 7.

Table 8. Calculated Values of Selected Solid-Vapor Surface Energies

Element	Z	T_m (°C)	$\gamma_{lv}^{exp}(T_m)$ J/m² a)	RT_m/A (J/m²)	$\sigma_{sv}(T) = X(RT_m/A) + \sigma_{sv}(T_m)$ J/m² b)			
					25°C	200°C	350°C	500°C
Li	3	180.5	0.398	4.99×10^{-2}	0.494	NA	NA	NA
Na	11	97.8	0.191	2.80×10^{-2}	0.234	NA	NA	NA
Si	14	1410	0.730	19.95×10^{-2}	1.041	1.027	1.011	0.995
K	19	63.7	0.101	1.62×10^{-2}	0.122	NA	NA	NA
Cr	24	1875	1.700 c)	35.15×10^{-2}	2.331	2.312	2.294	2.273
Cu	29	1083	1.300	22.48×10^{-2}	1.730	1.707	1.685	1.664
Ag	47	960.8	0.920 c)	15.98×10^{-2}	1.223	1.204	1.188	1.167
Au	79	1063	1.140	17.38×10^{-2}	1.496	1.476	1.460	1.444

a) L. E. Murr, Interfacial Phenomena in Metals and Alloys, Addison-Wesley Publishing Co., Reading, Massachusetts (1975), 101-106.

b) Values calculated using the method of W. R. Tyson and W. A. Miller, Surf. Sci., 62 (1977) 267-276.

c) W. R. Tyson and W. A. Miller, Surf. Sci., 62 (1977) 267-276.

The σ_{sv} for the Au-Cu alloys is always lower than pure Au or pure Cu and γ_{lv} for the Au-Ag alloys (where the dependence of σ_{sv} on γ_{lv} has already been described) is highest for Au and continuously decreases with increasing amounts of the lower surface energy component, Ag.

It is acknowledged, however, that these calculations indicate that Cr should increase the solid-vapor surface energy of Au, making its out-diffusion thermodynamically unacceptable with respect to the solvent. G. C. Nelson and P. H. Holloway[73] show this not to be the case. C. A. Chang[34] observes easy diffusion of both Cr and Si through gold thin films, again in contrast to surface energy criteria. These discrepancies are lessened with the realization that each metallurgical system responds in varying degrees to the driving forces for system energy reduction. Because the surface energies of both Cr and Si are comparable to that of Au (in contrast to the values attributed to Li, Na and K), their out-diffusion may have little influence upon altering the solid-vapor energy of the Au film itself. Their out-diffusion will, however, lower the energy of the system with respect to the solutes' activities, making the chemical potential gradient the primary driving force in Cr- and Si-contaminated Au thin films. The authors that documented the out-diffusion of Cr[34,73] and Si[34] were not concerned with an examination of the Au surface itself after out-diffusion of the solutes. This implies that surface degradation, originating from surface energy reduction through solute adsorption, as seen in this work was not evident.

Notwithstanding, surface energy criteria must be invoked to describe the severe and rapid degradation of Au films containing alkali impurities when compared to pure Au films. Calculated values of the alkali elements' σ_{sv}'s based upon experimental γ_{lv} values indicate that additions of the alkali elements are likely to reduce the surface and grain boundary energies of Au. Surface energy requirements could, then, describe the grain boundary grooving and hole formation in alkali-doped Au films after moderate isothermal heat treatments and the anode failures catalogued after dc stressing.

Values for the liquid-vapor surface energies of Li_2O, Na_2O and K_2O--which would more accurately depict the species adsorbed along the Au surface--are unavailable.

6.6 The Effect of Adsorption on Surface Diffusion

While the driving force for groove production at elevated temperatures is surface energy reduction, the rate at which a groove forms depends upon the method of mass transfer. In the temperature range examined here, all diffusion modes but bulk diffusion should be operative. For isothermally annealed Au, surface diffusion is competitive since (even at high temperatures) oxygen adsorption is known to retard Au's surface diffusion as measured by a slower grain boundary grooving rate,[51] which underscores the resistance of pure Au films to grain boundary grooving during heating and dc stressing tests noted in this work.

As a final suggestion for describing the rapid grain boundary grooving observed in alkali-doped Au thin films, it is noted that H. P. Bonzel[91] asserts that D_s can be increased or decreased as a function of adsorbate type and form. Qualitatively, the researcher has observed[92] for a number of metals including gold, that as the adsorbate's melting point decreases, the surface diffusion of the metals increases, since the adsorbate is less strongly tied to the materials' defects. Carbon, for example, reduces the surface diffusion coefficient in Cu[93] and Au[94] while Cl markedly increases D_s in Cu.[95] While this observation is only empirical, it does seem likely that the alkali elements, which are all liquid below 200°C, could enhance Au surface diffusion upon adsorption, thereby accelerating groove production. Au surface diffusion would be reduced with Cr and Si adsorption due to their high melting points.

CHAPTER 7
SUMMARY DISCUSSION

7.1 Review of Present Work in Relation to Other EM Studies

It is well accepted that the charge carrier/diffusing atom interaction dominates the electromigration behavior of most metallic systems.[30,96] This requires anode-directed atom migration in electron conductors and cathode-directed migration in hole conductors. It is also expected that any alloying elements migrate in the same direction as the matrix atoms,[97] that is, the effective charges, Z*'s, of both solvent and solute generally have the same polarity. In Table 9 several examples of experimentally determined Z* values as well as other electromigration characteristics for gold are listed, where electron wind-directed flow is designated in Table 9 by a negative Z* value. (A negative effective charge is synonymous with anode-directed migration in electron conductors.) The magnitude of Z* varies extensively because its value is determined by the competition between the electron wind and electrostatic forces which are both based upon numerous material characteristics, the experimental conditions and the theoretical model chosen (See Sections 2.2 and 2.3.2). In spite of the wide variation in the magnitude of the effective charge, however, its polarity is always negative.

It has typically been the case that a qualitative determination of the Z* polarity could be understood by examining film samples that had failed by electromigration. The location of the open so-produced indicates the sample position from where material has been depleted. In the

Table 9. Experimental Electromigration and Associated Diffusion Parameters Pertinent to Gold

Solute/Solvent	T (^{o}C)	Exp. Method J (Amps/cm^2)	Diffusion Coefficient D_b^0(cm^2/s)/δD_{gb}^0(cm^3/s)	 Q_{Diff}(eV)	Q_{EM}/EM Direction/Z*
^{198}Au/99.99% single crys. Au[a)]	286-412	Tracer, electrochem. sect.	$D_b^0 = 0.026 {}^{+0.034}_{-0.015}$	1.73 ± 0.04	---
Au/99.97% Au rod[b)]	850-1000	Marker motion $\simeq 10^4$	---	---	anode $-8.3 < Z^* < -5$
^{195}Au/99.999+% polycrys. Au rod[c)]	367-444	Tracer & rf backsputt.	$\delta D_{gb}^0 = 3.1 \times 10^{-10}$	0.88 ± 0.02	---
Au/polycrys. Au film[d)]	202-293	Lifetime 6.0×10^6	---	0.88 ± 0.06	0.88 ± 0.06 anode
^{195}Au/e-beam Au films[e)]	120-250	X-stripe SEM, audiorad. $0.8\text{-}3.0 \times 10^6$	---	0.8 ± 0.03	0.8 ± 0.03 anode $-89 < Z^* < -20$
Au/evap. Au films[f)]	250-390	Resistometric 6.0×10^5	---	---	0.98
^{22}Na/99.99% polycrys. Na[g)]	0-97	Tracer Serial sect.	$D_b^0 = 0.145$	0.438	---
Na/Na[h)]	88-93	Marker motion	---	---	0.42 ± 0.03 anode $Z^* \simeq -(2.4 \pm 0.5)\lvert e \rvert$

a) W. Rupp, U. Ermert and R. Sizmann, Phys. Stat. Sol., 33 (1969), 509-516.
b) H. B. Huntington and A. R. Grone, J. Phys. Chem. Solids, 20 (1/2) (1961), 76-87.
c) D. Gupta, J. Appl. Phys., 44 (10) (1973), 4455-4458.
d) A. Gangulee and F. M. d'Heurle, Scripta Met., 7 (1973), 1027-1030.
e) K. L. Tai and M. Ohring, J. Appl. Phys., 48 (1) (1977), 36-45.
f) R. E. Hummel and H. J. Geier, Thin Solid Films, 25 (1975), 335-342.
g) J. N. Mundy, L. W. Barr and F. A. Smith, Phil. Mag., 14 (1966), 785-802.
h) G. A. Sullivan, Phys. Rev., 154 (1967), 605-613.

case of electron wind-directed EM, the open generally occurs at the cathode with material accumulation at the anode. The use of failure site location as an indicator of Z* polarity, however, requires precise knowledge that electromigration is indeed the predominant failure mechanism. In addition, while EM failures may consistently occur in the "cathode portion" of the powered stripe, the exact location is a function of the temperature profile (See appendix) and local structural inhomogeneities.

Given this common procedure for determining migration direction it was difficult to apply electron wind arguments to the EM failure results for Au films studied by R. E. Hummel and H. M. Breitling in 1971[1] and by R. E. Hummel and H. J. Geier in 1975.[98] These researchers found for gold films deposited on laboratory grade microscope slides that EM-induced failure was routinely located near the anode portion of the stripe. In the latter study the activation energy for Au electromigration by way of grain boundary diffusion was determined and compared to that observed by other film researchers.[98] While the value of the activation energy for the process, Q_{Au}^{EM} = 0.98 eV, compared favorably with the results of others (See Table 9), their determination of the failure site location could not be reconciled with those who had observed failure in Au thin films relegated to the cathode portion of the stripe.[14,99]

I. A. Blech and R. Rosenberg conducted a study[100] during which pure gold films deposited on Na-glass substrates and Au + Co films deposited on Na-glass substrates were seen to fail at the anode, but when both film types were annealed in 150°C air/15.0 hr, followed by 150°C vacuum/ 15.0 hr, the samples failed at the cathode. I. A. Blech and R. Rosenberg intimated that the complicated film configuration used by R. E. Hummel et al.[1,98] led to anode failure due to overlooked structural inhomogeneities in the films that were corrected with annealing and that uniform Au films would fail at the cathode. In 1977, K. L. Tai and M. Ohring[39] reiterated this belief in observing that the migration of ^{195}Au tracer atoms in Au films was anode-directed whether a Mo adhesive was used or not.

Meanwhile, R. E. Hummel, B. K. Krumeich and R. T. DeHoff in 1978[101] showed using AES that measurable amounts of sodium could be detected on the surface of a 1000 Å Au film deposited on Na-glass after moderate annealing. Further study of the low temperature diffusion of sodium through Au films verified that sufficient Na had diffused through an 800 Å film on Na-glass after 150°C air/5 min to be visible with AES. Whether such out-diffusion of Na actually affected gold electromigration was not yet determined.

The original impetus for this work stemmed from a need to clarify these experimental discrepancies. The use of three types of borosilicate ribbon, each containing 7.5 mole% of either Li_2O, Na_2O or K_2O, allowed for the examination of electromigration in 800 Å gold thin films as affected by alkali impurities.

The alkali elements, being only loosely tied to the borosilicate matrix, migrate to the Au/glass interface to eliminate defects there and enter the film in response to an initial driving force caused by the chemical potential difference of the solute between the two gold surfaces. This out-diffusion is promoted by the moderately high temperatures generated in the sample during current stressing. Once in the film, the alkali impurities migrate via the film's grain boundaries, where they are acted upon by a variety of forces.

In order to separate the effects produced by the application of an electric field from those effects arising solely from the associated resistive heating caused by this electric field, a study of samples subjected to isothermal heat treatments was conducted. The temperatures of the heat treatments were chosen to approximate the temperatures encountered by the stripe during EM stressing at 1 Amp powering, i.e., a current density of $\simeq 8.0 \times 10^5$ Amps/cm^2.

Gold films deposited on all three alkali borosilicate glasses experienced marked grain boundary grooving at moderate annealing temperatures for short times in contrast to Au films on quartz slides annealed under similar conditions (Compare Figure 1 with Figures 4, 5 and 6).

Gold films deposited on high purity quartz exhibited only slight grain boundary grooving at the temperatures encountered. Since the samples were annealed at a pressure of 1 Torr, impurity adsorption along the surface occurred. Oxygen adsorption on pure Au is known to reduce D_s, thereby reducing the degree of grain boundary grooving.[51] The grooves formed were first visible after an anneal of 340°C/3 hr only at high magnification (20 kX) and at this temperature did not act as nucleation sites for through-holes. Some hole formation was observed after a heat treatment of 560°C/1 hr, but a number of these holes were due to isolated defects such as sites of trapped gases.

In contrast, 800 Å gold films deposited on all three types of alkali borosilicate glass experienced severe surface roughening beginning at low temperatures (200°C/5 hr). The holes formed and grain sliding adjacent to the holes were seen in all three types of alkali-doped Au films. Hole size density continually increased for Li-doped and Na-doped

Au films up to heat treatments of 500°C/5 hr. While the hole density increased in the K-doped Au films during the same heat treatment, the hole size stabilized after 350°C/5 hr.

The high degree of overall surface degradation in the alkali-contaminated films is endemic of a complex surface energy reduction process. Since the temperature range used and the large grain boundary and surface areas inherent to thin films cause grain boundary diffusion of the solutes to be the predominant mass transfer mechanism, the film degradation during annealing must be the effect of alkali out-diffusion along the film's grain boundaries coupled with its collection along the surface of the film. For K and Na, where no solubility occurs with Au in the solid state,[63,102] grain boundaries offer the only viable migration paths.

Since the surface energies for the alkali elements, as calculated from γ_{lv} measurements (See Section 6.5) are 3 to 12 times smaller than the same for Au at room temperature, it is expected that as the alkali ions out-diffuse, thereby coating the film grain boundaries, the interfacial energies of these boundaries will be reduced. At the same time the solid-vapor surface energy of the Au films is similarly reduced. Although it cannot be ascertained whether the alkalies remain pure in the grain boundaries or otherwise, it is reasonable to suggest that the Au surface is covered with some form of oxide, based upon the free energy of formation calculations presented in Table 6. While γ_{lv} and σ_{sv} values for the alkali oxides are not available, partial molar surface tension values for the class of oxides[103] suggest that low surface energies should be associated with both the pure and the oxide forms of the alkali elements.

Initially grooves form due to random impurity adsorption. With time, the alkali species migrates to the surface where it oxidizes. The surface energy decreases faster than γ_{gb}, despite γ_{gb} being less than the grain boundary interfacial energy of pure Au. By continously eliminating the higher energy grain boundary surface, large through-holes are rapidly produced in the alkali-contaminated Au films. The enhanced rate of film degradation occurs because the rate of mass transfer along the surface, D_s, is increased due to alkali adsorption. (The alkali elements are low melting.[92]) The grain sliding that occurs adjacent to a number of the holes is not understood at present, but may be due to some local, unanticipated surface contamination that keeps σ_{sv} of certain Au grains high. In order to test these postulates quantitatively, precise groove measurements are required.

These thermally-induced effects occur in similar alkali-doped Au stripes when the stripes are subjected to dc stressing.

An SEM examination of Au films deposited on either pure quartz or on alkali borosilicate ribbons that were current stressed indicated the following:

1) Sample failure location

   a) Au films deposited on pure quartz slides showed sign of cathode failure but were highly resistant to EM damage when compared to Au films on alkali borosilicate ribbons. Little EM-induced damage was evident after comparatively high current densities and long stressing times. Minor grain delineation in the cathode region due to Au depletion was noted.

   b) The majority of Au films deposited on Li-borosilicate glass exhibited holes at the anode. Even when actual failure occurred elsewhere along the stripe (Figure 11), a dense region of holes was visible at the anode even at low optical magnification.

   c) Failures of Au films on Na-borosilicate were located at either the anode or the cathode after dc current passage. The character of failure differed as a function of location.

   d) Au films deposited on K-borosilicate showed signs of failure predominantly at the anode. The character of grain boundary grooving and hole formation at the anode most strongly paralleled that seen for similar samples after isothermal heat treatment.

2) Sample failure character

   a) The character of anode failure in Au films deposited on all three types of borosilicate glass after current passage resembled the degradation of these films after annealing.

   b) The character of cathode failure in Au films on quartz and on alkali borosilicate slides was identical to 'typical' EM failure. The holes were elongated and many holes had adjacent hillock formation, indicating that local flux divergencies caused by the grain size variation throughout the film volume allowed for electron wind-induced mass transfer of the matrix material.

AES analysis of 800 Å Au films deposited on K-borosilicate ribbons that were removed from current stressing prior to discernible hole formation revealed that the maximum K distributions across the films were skewed towards the anode portion of the stripes with a maximum of surface potassium also apparent at the center of the stripes. This demonstrates the competition of electronic and thermal effects. A high K concentration relative to the rest of the sample was never observed at the cathode. AES analysis of an as-deposited film (aged for 30 days at 25^oC) produced no measurable K signal along the entire length of the film.

Several conclusions are drawn from these observations. First, and foremost, during the electromigration process in thin Au films, the nonrandom mass transfer of Au^+, Li^+, Na^+ and K^+ ions is induced primarily by the electron wind. This was seen experimentally as anode-directed mass transfer of both solute and solvent in Au, and that in all cases, the sign of the effective charge of each type of migrating ion, Z_i^*, is qualitatively negative. Anode-directed mass transfer of Au^+ ions in Au has been observed by many researchers for both bulk[27,104] and thin film[14,39,99] Au (See Table 9). Na^+ electromigration in bulk Na at low temperatures has also been verified to be anode-directed.[105] R. S. Sorbello[30] has noted through calculations of the force on impurities that are treated as several types of defects that for Li^+ in Li, Na^+ in Na, K^+ in K, Au^+ in Au and Li^+ in Au the dominating force on the migrating ion is in the direction of electron flow and increases with atomic number. W. Mock, Jr.,[68] found for resistively heated bulk Au, the EM of ^{125}Sb was controlled by the electron wind and that Sb diffusion was an order of magnitude more rapid than Au in Au in the temperature range of 750-850°C. The results of this work, R. S. Sorbello's calculations[30] and the investigation of W. Mock, Jr.[68] indicate that at least for Au, alloying elements migrate in the same direction as the matrix ions.[99]

Failure at the cathode was directly catalogued in this study for pure Au and some Na-doped Au films. As anode-directed flow of both loosely bound matrix ions and alkali solutes occurs, a simultaneous cathode-directed flow of vacancies occurs. Whether these flows occur on a local scale (structural divergencies) or on a global scale (temperature profile along the length of the stripe), this vacancy flow nucleates voids which connect to eventually form through-holes at the cathode and final failure.

In the case of alkali-doped Au films, the electron wind sweeps both solvent and solute towards the anode. Cathode damage, as seen in this study in all three types of alkali-doped Au films, is still caused by the vacancy flow towards the cathode. The ion and vacancy flows are driven by the electrical potential gradient across the length of the stripe that is activated by the application of an electric field during dc current passage. Whether the vacancy flow due to alkali introduction is greater than that of pure Au is uncertain, since the alkali impurities are initially not integral parts of the film boundaries and as interstitial defects, their effect on Au vacancy flow is at least complex.

An alternate failure mechanism is available in the alkali-doped Au films. There is an additional chemical potential gradient with respect to the alkali solute that is perpendicular to the plane of the film's external surface. During current powering this gradient will be reduced somewhat by the out-diffusion of the solute species to the Au surface. If processes such as oxidation effectively remove the species from the end of the diffusion path, however, the chemcial potential gradient will not be reduced and out-diffusion continues at a rapid rate.

Based upon these two gradients, an intermediate/final state of an alkali-doped Au film would include a distribution of alkali along the film surface with additional build-up of alkali at the anode after some time of current stress. The two gradient reduction processes, however, do not completely describe the failures seen in this work. While mass transfer is being driven by the chemical and electrical potential gradients, the nature of the alkali elements is such that their collection along the various gold surfaces produces severe grain boundary grooving and hole formation caused by a reduction in those surfaces' energies through alkali contamination. Since the alkali constituents are swept by the electron wind to the anode, once a minimum concentration of alkali is reached there, film degradation occurs rapidly.

Alkali accumulation at the anode produced the majority of failures in Li-doped and K-doped Au films examined in this study. Anode failure in alkali-doped films is not evidence of matrix material depletion but rather solute accumulation.

A critical concentration of alkali impurity, specific temperature range or current density was not noted that separated anode failures from cathode failures. A demarcation between failure types cannot be made for several reasons. Alkali out-diffusion may be a strong function of grain boundary structure. Whether alkali motion is parallel or perpendicular to the film surface depends upon the binding energy of a particular Au plane and the location of a neighboring vacancy on or near that plane. The non-uniformity of alkali distribution in the borosilicate substrate may partially explain the two types of potassium profiles seen in the AES results and the variation in failure location. Alkali-doped Au films did have a tendency to fail sooner than pure Au, which might indicate that the activation energy for grain boundary diffusion of the alkali impurities in Au is less than that of Au in Au, but the decision to fully examine each sample used in this work prevented the collection of a large set of sample failures as is necessary for suitable MTF studies.

7.2 Additional Considerations

Areas that warrant further investigation can be broadly grouped into either the study of materials produced in thin film form or the electromigration behavior of such materials. It has been suggested (See Section 2.3.1) that a number of theoretical and experimental difficulties specific to thin films exists. Basic property relationships such as the effect of film grain size and orientation on thin film resistivity have been modeled to include grain boundary and surface scattering[106,107] but such models are not often incorporated in the theoretical treatments of processes such as electromigration. The statistical nature of grain boundaries and concomitant film property changes as a function of grain boundary structure and orientation have fundamental effects upon electromigration and, while grain boundary diffusion parameters are difficult to determine quantitatively, these parameters need to be evaluated. The importance of the film/environment and film/substrate interfaces cannot be overstressed. These interfaces must be considered more fully as parts of the thin film system which may require the re-evaluation of the boundary conditions used to model grain boundary diffusion and EM.

The transition from bulk models describing electromigration to thin film models is not easy. Analysis of EM based upon the standard steady state flux equations[97] predicts that Cu additions to Al should enhance vacancy flow and thereby increase EM in 4%Cu-Al metallizations, which directly contrasts the EM behavior actually observed in thin films of this composition.[108]

Surfaces suddenly play a large role in film behavior and their surface structure, impurity adsorption characteristics, etc. are not well known. As has been shown in this work, until fundamental thin film properties can be more fully appreciated and quantified, the interpretation of the electromigration and of other processes can prove difficult.

There are many areas of interest specific to the research presented here. If electron beam effects that alter the migration of the alkali elements[48] can be remedied, a uniform method of alkali introduction discovered and the degree to which atmospheric adsorbates such as C, O_2 and

S affect alkali out-diffusion clarified, quantitative AES is warranted. The grain boundary diffusion parameter, $K\delta D_{gb}$, could then be determined, using, for example, the surface accumulation analytical technique of J. C. M. Hwang and R. W. Ballufi[109] for solutes exhibiting negligible leakage into the bulk. Such analysis would offer insight into the degree of competition between alkali accumulation and Au depletion. This information combined with surface energy data could lead to the description of grain boundary structure, impurity binding energies and possible orientations that might inhibit electron wind-induced mass transfer. Such information would also aid in defining the general role grain boundaries have in controlling a variety of thin film processes.

Is the list of competing mechanisms endless? Has the ambient been often considered in activating a presumably dormant mechanism? Is it important to know which of the alkalies produces the most severe grain boundary grooving and EM damage in gold? How do Au grain boundaries with solutes scatter electrons when compared to their pure counterparts? The answers to such questions have broad implications for the general class of thin film materials.

While it has long been recognized that from a practical standpoint the addition of appropriate solutes and the modification of grain boundary triple point divergencies by altering grain boundary orientations with or without solutes[110] were the most likely methods to prohibit thin film EM, new developments such as the 'bamboo structure'[111] offer completely new approaches for improving EM resistance in metallizations. The researchers who observed this structure[111] found that 0.5%Cu-Al stripes exhibited increased EM resistance as their linewidths were reduced from 2 to 1 microns. SEM analysis showed that an entirely new morphology was produced during the deposition of the narrower stripes such that the films' grains were of uniform size and the grain boundaries were perpendicular to current flow. This study reveals not only the crucial relationship between processing and film properties but demonstrates that decreasing linewidths do not necessarily promote reduced EM resistance.

Theoretically, new models such as that presented by S. T. Pai and J. P. Marton,[26] while still maintaining that the effective charge determines the degree and polarity of electromigration, focus on additional material constants that may prove critical in finally determining the fundamental interactions that define the general EM process.

It is hoped that the work presented here demonstrates that as a thin film metallization is dc powered, a number of competing processes occur. Each migration process interacts with all others in a complex way, making analysis of the effects of one process difficult to isolate from those of all other processes. Experiments can be designed, however, to reduce the contribution of these latter processes. While such studies ignore the coupling of the processes active under normal conditions, they can indicate which mechanisms are likely to predominate.

It is also hoped that the research discussed here illustrates that, without a broad understanding of the complexity of thin film properties, the examination of a specific process such as electromigration may prove frustrating.

Continued study of the electromigration behavior in thin films remains timely, particularly when the recent observation of electromigration in p-type semiconductors[112] is considered and the continued miniaturization of microelectronic components is acknowledged.

APPENDIX
INDICATION OF COMPETING MECHANISMS DURING DC STRESSING

It became apparent during the early stages of experimentation that a number of parallel processes occur within a metallic stripe that is powered by a dc current. In addition to electromigration, these thermally-activated processes persist in direct response to the resistive heating of the metal during powering. Since these processes--chemical potential reduction of the solute, grain boundary grooving, thermotransport, etc.--are dependent upon diffusion of the stripe's constituents, as is EM, all have some probability of producing film failure.

An examination of two thin film compositions indicate that, for a given experimental program, these films can fail for different reasons. Figure A-1 contrasts the failure of pure gold films with that of gold films deposited on an intermediate layer of 135 Å of indium which is catalogued in Figure A-2. All samples were mounted on a ceramic sample holder and subjected to a dc current. The pertinent experimental parameters for each sample are listed in the figures.

To verify that failure location in these samples was not merely a function of sample configuration, two different film patterns were tested for each composition. By altering the line pattern in some of the samples, the temperature distribution across the film length could be manipulated. The temperature distributions generated by the associated film patterns are depicted schematically in the figures.

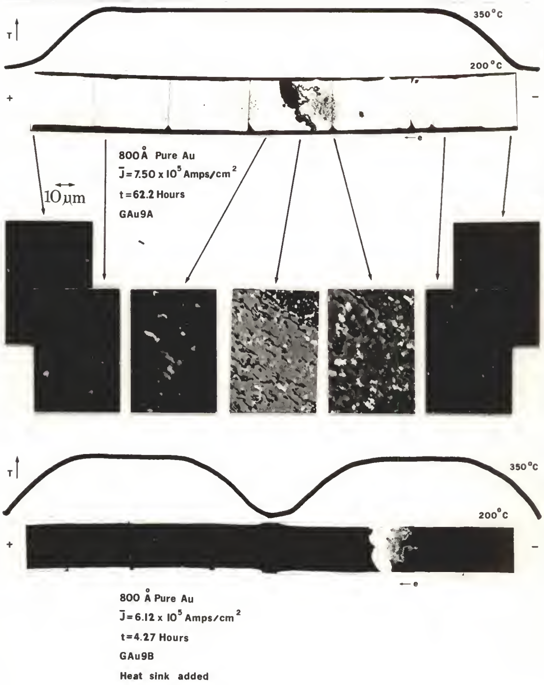

Figure A-1. Failure Location Variation in Pure Au Films as a Function of Maximum Temperature Location.

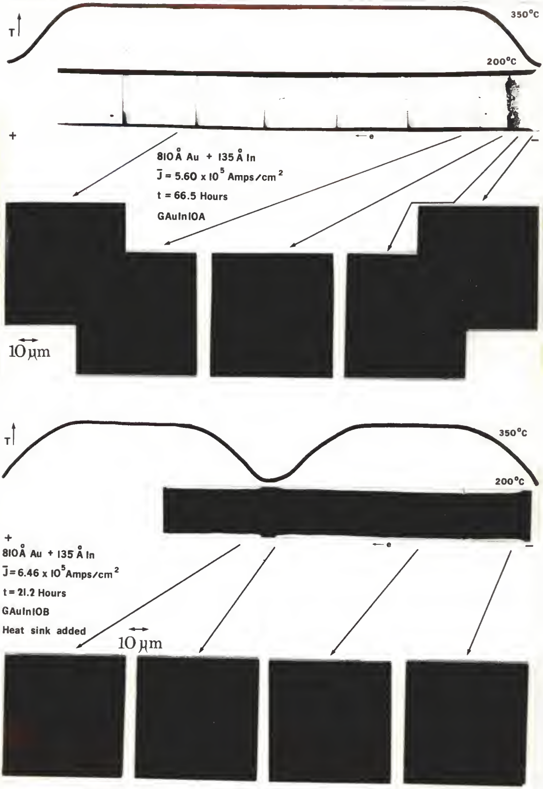

Figure A-2. Electromigration Failure Location Variation in Au Films on Intermediate In Adhesion Layer as a Function of Maximum Temperature Location.

During dc stressing, electrons flow from cathode to anode. Simultaneously, a parabolic temperature profile is induced along the metallization due to Joule heating, with the central portion of the sample experiencing the maximum absolute temperature.[27,112] Any perturbation along the stripe's length alters the temperature distribution. This is the case for the second film pattern used in this study. The electrode added to the center of the stripe line aids heat dissipation to such a degree that the film in this pattern experiences a double parabolic temperature profile. This electrode/heat sink also increases the temperature gradient across the stripe as a function of position. Finally, this film configuration changes the position of the maximum absolute temperature to positions 25% and 75% across the sample length.

Failure due to temperature-induced grain boundary grooving of the pure film material is relegated to areas along the stripe where the absolute temperature is a maximum. Failure due to electromigration often occurs where the temperature gradient is a maximum.[110] These EM failures are found near one of the electrode/heat sink edges as determined by the sign of the effective charge, Z*.

After subjecting pure Au and Au on In samples to a dc current, evidence of failure was noted by observing the stressed films with an optical microscope at 30X magnification and in a scanning electron microscope (SEM) at 500/1000X magnification.

Examination of the micrographs in Figure A-1 show that pure Au films failed in this initial study primarily due to accelerated grain boundary grooving for this specific experimental program. In both sample configurations--with or without the additional heat sink--pure gold samples exhibited hole formation, hole coalescence and eventual failure at positions of highest temperature. The failure in the heat-sinked sample occurred at the position 75% across the length of the sample as expected for the double temperature profile configuration. Whether the sample fails at 25% or 75% is only a statistical matter. The pure Au film without the heat sink lasted longer than its heat-sinked counterpart while experiencing a higher current density due to the reduced severity of the temperature profile in the former configuration.

The SEM micrographs of the designated film areas corroborate the optical scans, showing an increase in the number and size of film holes as the absolute temperature increases towards the center.

In contrast, the predominant failure mechanism for the gold on indium samples (Figure A-2) is electromigration. Regardless of the sample heat sink configuration, failure occurs in the region of the largest temperature gradient and near the cathode. The higher number of grain boundaries in the fine grained gold on In promoted atom diffusion via these boundaries when compared to the gold films deposited on quartz. The failure typifies that due to electron wind-directed EM.

Several observations were made during this preliminary work:

1) The predominance of one failure mechanism over another during dc stressing changes with the metallurgical system examined. If the primary failure mechanism has not been pinpointed, the reduction of one mechanism may not reduce the overall failure rate of that system. Also, the reduction of one failure mode may or may not enhance another.

2) While all of the aforementioned processes have some probability of producing failure, a properly designed experiment can accentuate the mechanism of interest. In the work reported here, a change in sample holder from ceramic to metal produces a change in the dominant failure mechanism of pure Au films from temperature-induced grain boundary grooving to electromigration.

3) The need for a uniform procedure for dopant introduction into gold films was noted. While it was the intent of this work to use the indium layer as a source of diffusant, the use of such intermediate layers to promote Au adhesion,[12,73] to act as an electroplating base,[13] or a diffusion barrier[113] is well documented. Such intermediate films were deemed inappropriate for future work, since such effects are relatively independent of solute species.

REFERENCES

1. R. E. Hummel and H. M. Breitling, Appl. Phys. Lett., 18 (9) (1971), 373-375.

2. I. A. Blech and H. Sello, Physics of Failures in Electronics, vol. 5, Rome Air Development Center, USAF (1966), 496.

3. A. R. Grone, J. Phys. Chem. Solids, 20 (1/2) (1961), 88-93.

4. K. H. Kraatz, G. Frohberg and H. Wever, Phys. Stat. Sol. (a), 52 (1979), 149-159.

5. H. R. Patil and H. B. Huntington, J. Phys. Chem. Solids, 31 (1970), 463-474.

6. D. A. Golopentia and H. B. Huntington, J. Phys. Chem. Solids, 39 (1978), 975-984.

7. C. Herzig and H. E. Peltner, Phys. Stat. Sol. (a), 47 (1978), 497-508.

8. H. Nakajima and K. Hirano, J. Appl. Phys., 48 (5) (1977), 1793-1796.

9. I. A. Blech and E. S. Meiren, J. Appl. Phys., 40 (2) (1969), 485-491.

10. F. M. d'Heurle and I. Ames, Appl. Phys. Lett., 16 (2) (1970), 80-81.

11. S. T. Pai, J. P. Marton and D. C. Beatty, Can. J. Phys., 55 (1977), 116-128.

12. J. C. Blair, C. R. Fuller, P. B. Ghate and C. T. Haywood, J. Appl. Phys., 43 (2) (1972), 307-311.

13. A. Gangulee and F. M. d'Heurle, Scripta Metall., 7 (10) (1973), 1027-1030.

14. T. E. Hartman and J. C. Blair, IEEE Trans. Electronic Devices, ED-16 (4) (1969), 407-410.

15. P. H. Sun and M. Ohring, J. Appl. Phys., 47 (2) (1976), 478-485.

16. G. J. van Gurp, Thin Solid Films, 38 (1976), 295-311.

17. J. R. Lloyd, M. R. Polcari and G. A. MacKenzie, Appl. Phys. Lett., **36** (6) (1980), 428-430.

18. D. T. Peterson, in *Electro- and Thermo-Transport in Metals and Alloys*, edited by R. E. Hummel and H. B. Huntington, Amer. Inst. of Mining, Metallurgical and Petroleum Engineers, Inc., New York (1977), 54-67.

19. M. J. Attardo and R. Rosenberg, J. Appl. Phys., **41** (6) (1970), 2381-2386.

20. J. R. Black, Proc. of the IEEE, **57** (9) (1969), 1587-1594.

21. R. S. Sorbello and B. Dasgupta, Phys. Rev. B, **16** (12) (1977), 5193-5205.

22. H. B. Huntington, M. D. Feit and D. Lortz, Crystal Lattice Defects, **1** (1970), 193-200.

23. V. B. Fiks, Soviet Phys.: Solid State 1, **14** (1959), 14-28.

24. G. J. van Gurp, J. Phys. Chem. Solids, **38** (1977), 627-633.

25. Substitution of E_F (Au at 25°C) = 5.51 eV into equation (4) and equation (5) and noting that ρ (Au at 25°C) = 2.44×10^{-6} Ω-cm = $m_e/ne^2\tau$ gives $\vec{p}_F > 10^7 \Delta\vec{p}$.

26. S. T. Pai and J. P. Marton, Can. J. Phys., **55** (1977), 103-115.

27. H. B. Huntington and A. R. Grone, J. Phys. Chem. Solids, **20** (1/2) (1961), 76-87.

28. H. B. Huntington, in *Diffusion in Solids: Recent Developments*, edited by A. S. Nowick and J. J. Burton, Academic Press, Inc., New York (1975), 306.

29. C. Bosvieux and J. Friedel, J. Phys. Chem. Solids, **23** (1962), 123-136.

30. R. S. Sorbello, J. Phys. Chem. Solids, **34** (1973), 937-950.

31. R. S. Sorbello, in *Electro- and Thermo-Transport in Metals and Alloys*, edited by R. E. Hummel and H. B. Huntington, Amer. Inst. of Mining, Metallurgical and Petroleum Engineers, Inc., New York (1977), 11.

32. A. K. Das and R. Peierls, J. Phys. C, **8** (1975), 3348-3351.

33. L. J. Sham, Phys. Rev. B, **12** (8) (1975), 3142-3149.

34. C. A. Chang, J. Electrochem. Soc., **127** (6) (1980), 1331-1334.

35. M. H. Fariàs, J. L. Peña and F. Sánchez-Sinencio, J. Vac. Sci. Technol., 21 (3) (1982), 853-857.

36. P. S. Ho, F. M. d'Heurle and A. Gangulee, in Electro- and Thermo-Transport in Metals and Alloys, edited by R. E. Hummel and H. B. Huntington, Amer. Inst. of Mining, Metallurgical and Petroleum Engineers, Inc., New York (1977), 111.

37. R. Rosenberg, in Nature and Behavior of Grain Boundaries, edited by Hsun Hu, Plenum Publishing Corp., New York (1972), 331.

38. P. S. Ho and J. K. Howard, J. Appl. Phys., 45 (8) (1974), 3229-3233.

39. K. L. Tai and M. Ohring, J. Appl. Phys., 48 (1) (1977), 36-45.

40. P. S. Ho, J. Appl. Phys., 49 (5) (1978), 2735-2742.

41. G. Martin, Phys. Stat. Sol. (a), 14 (1972), 183-190.

42. R. T. Whipple, Philos. Mag., 45 (1954), 1225-1236.

43. Borosilicate ribbons were made to order by Specialty Glass, Inc., Oldsmar, Florida. The raw materials included high purity Custer 30F sand (SiO_2), U. S. Borax technical grade boric acid (B_2O_3) and technical grade alkali oxide materials. The constituents were melted together at 1450°C in a high purity silica crucible for about two hours and then transferred to another fused silica draw crucible for rapid quenching by drawing into rod. All rods were fire refined to produce a semiconductor smooth finish.

44. R. W. Petticrew, personal communication.

45. R. T. DeHoff, personal communication.

46. D. M. Mattox, Thin Solid Films, 53 (1978), 81-96.

47. L. L. Hench, personal communication.

48. P. H. Holloway, personal communication.

49. K. L. Chopra, Thin Film Phenomena, McGraw-Hill Book Co., New York (1969), 62.

50. W. A. Slippy, Jr., Master's Thesis, University of Florida (1969).

51. G. Neumann and G. M. Neumann, in Surface Self-Diffusion of Metals, Diffusion Monograph Series edited by F. H. Wöhlbier, Diffusion Information Center, Bay Village, Ohio (1972), 61.

52. Ibid., 63.

53. Based upon stereological considerations, the area of film covering an area of substrate is equal to the number of points of a properly constructed grid in the film divided by the total number of points.

54. R. P. Elliot, Constitution of Binary Alloys, 1st supplement, McGraw-Hill Book Co., New York (1965), 93.

55. Lambda Electronics regulated power supplies, model LPT-7202-FM, rated at 0-20 V ± (0.01% + 1.0mV), 0-1.5 Amps ± 0.2%.

56. Yokogawa Electronics Works, Ltd. 6-point strip chart recorder, model ER106-G, rated at 0.005-25.0 V ± 0.5%, 2.5 s (60 Hz).

57. JEOL JSM-35C scanning electron microscope.

58. N. C. MacDonald, Scanning Electron Microscopy/1971, IITRI, Chicago, Illinois (1971), 91.

59. J. I. Goldstein, in Practical Scanning Electron Microscopy, edited by J. I. Goldstein and H. Yakowitz, Plenum Press, New York (1975), 91.

60. N. A. Alford, A. Barrie, W. Drummond and Q. C. Herd, Surface and Interface Analysis, 1 (1) (1979), 36-44.

61. L. E. Davis, N. C. MacDonald, P. W. Palmberg, G. E. Raich and R. E. Weber, Handbook of Auger Electron Spectroscopy, 2nd edition, Phys. Elec. Div., Perkin-Elmer Corp., Eden Prairie, Minnesota (1976), 1.

62. M. Wuttig and H. K. Berenbaum, Phys. Rev., 147 (1966), 495-504.

63. R. P. Elliot, Constitution of Binary Alloys, 1st supplement, McGraw-Hill Book Co., New York (1965), 92.

64. By calculating the number of Au atoms in cubic grains 2000 Å on a side and noting the number of K atoms associated with the neighboring 10 Å grain boundaries, that there are 3.4 K atoms for every 1000 Au atoms can be determined.

65. P. H. Holloway, Scanning Electron Microscopy/1978, 1 (1978), 361-374.

66. F. Pons, J. LeHéricy and J. P. Langeron, Surf. Sci., 69 (1977), 547-564.

67. P. Légaré, L. Hilaire, M. Sotto and G. Maire, Surf. Sci., 91 (1980), 175-186.

68. W. Mock, Jr., Phys. Rev., 179 (3) (1969), 663-676.

69. T. Furukawa and W. B. White, J. Mat. Sci., 16 (1981), 2689-2700.

70. W. D. Kingery, H. K. Bowen and D. R. Uhlmann, Introduction to Ceramics, 2nd edition, John Wiley and Sons, Inc., New York (1976), 873.

71. K. K. Evstrop'ev and V. K. Pavlovskii, Inorg. Mater., 3 (1967), 592-596. Translated from Neorg. Mater., 3 (1967), 673-678.

72. W. Müller-Warmuth, F. Krämer and H. Dutz, IX^{2} Congrès Intern. du Verre, Versailles, Section AI.2 (1971), 303-318.

73. G. C. Nelson and P. H. Holloway, Surface Analysis Techniques for Metallurgical Applications, ASTM STP 596, Amer. Soc. of Testing and Materials (1976), 68-78.

74. G. H. Frischat, Ionic Diffusion in Oxide Glasses, Trans Tech Publications, Bay Village, Ohio (1975), 11.

75. G. Korányi, Surface Properties of Silicate Glasses, Hungarian Academy of Sciences, Budapest, Hungary (1963), 30.

76. Ibid., 80.

77. G. Keppeler and M. Hechter, Glast. Ber., 12 (11) (1934), 366-372.

78. T. von Takáts, Glast. Ber., 14 (3) (1936), 103-105.

79. C. G. Pantano, Jr., D. B. Dove and G. Y. Onoda, Jr., J. Noncryst. Solids, 19 (1975), 41-53.

80. L. L. Hench, "Ultrastructure Processing and Environmental Stability of Advanced Structural and Electronic Materials," 1st Annual Report to the Air Force Office of Scientific Research, Bolling Air Force Base, D. C. (1981), 23.

81. G. Korányi, Surface Properties of Silicate Glasses, Hungarian Academy of Sciences, Budapest, Hungary (1963), 86.

82. K. L. Chopra, Thin Film Phenomena, McGraw-Hill Book Co., New York (1969), 316.

83. Ibid., 318.

84. J. C. Fisher, J. Appl. Phys., 22 (1) (1951), 74-77.

85. J. C. M. Hwang, J. D. Pan and R. W. Ballufi, J. Appl. Phys., 50 (1979), 1349-1359.

86. R. A. Swalin, Thermodynamics of Solids, 2nd edition, John Wiley and Sons, Inc., New York (1972), 250.

87. W. W. Mullins, J. Appl. Phys., 28 (3) (1957), 333-339.

88. L. E. Murr, Interfacial Phenomena in Metals and Alloys, Addison-Wesley Publishing Co., Reading, Massachusetts (1975), 126.

89. W. R. Tyson and W. A. Miller, Surf. Sci., 62 (1977), 267-276.

90. W. R. Tyson, Can. Met. Quart., 14 (1975), 307-312.

91. H. P. Bonzel, in Surface Physics of Materials, vol. 11, edited by J. M. Blakely, Academic Press, Inc., New Yrok (1975), 317.

92. Ibid., 318.

93. H. P. Bonzel and N. A. Gjostein, in Molecular Processes on Solid Surfaces, edited by E. Drauglis, R. G. Gretz and R. I. Jaffee, McGraw-Hill Book Co., New York (1969), 544.

94. D. L. Olson, H. R. Patil and J. M. Blakely, Scripta Metall., 6 (1972), 229-240.

95. F. Delamare and G. E. Rhead, Surf. Sci., 28 (1971), 267-284.

96. H. B. Huntington, Trans. Metall. Soc. AIME, 245 (1969), 2571-2579.

97. P. S. Ho, Phys. Rev. B, 8 (10) (1973), 4534-4539.

98. R. E. Hummel and H. J. Geier, Thin Solid Films, 25 (1975), 335-342.

99. L. Berenbaum and R. Rosenberg, Thin Solid Films, 4 (1969), 187-204.

100. I. A. Blech and R. Rosenberg, J. Appl. Phys., 46 (2) (1975), 579-583.

101. R. E. Hummel, B. K. Krumeich and R. T. DeHoff, Appl. Phys. Lett., 33 (1) (1978), 960-962.

102. M. Hansen, Constitution of Binary Alloys, McGraw-Hill Book Co., New York (1958), 218.

103. J. J. Bikerman, Physical Surfaces, vol. 20, Physical Chemistry: A Series of Monographs edited by Ernest M. Loebl, Academic Press, Inc., New York (1970), 68.

104. H. M. Gilder and D. Lazarus, Phys. Rev., 145 (1966), 507-518.

105. G. A. Sullivan, Phys. Rev., 154 (1967), 605-613.

106. J. R. Sambles, K. C. Elsom and D. J. Jarvis, Phil. Trans. R. Soc. London A, 304 (1982), 365-396.

107. A. J. Tosser, C. R. Tellier and C. R. Pichard, J. Mat. Sci., 16 (1981), 944-948.

108. I. Ames, F. M. d'Heurle and R. Horstmann, IBM J. Res. Devel., 4 (1970), 461-463.

109. J. C. M. Hwang and R. W. Ballufi, J. Appl. Phys., 50 (3) (1979), 1339-1348.

110. R. Rosenberg, A. F. Mayadas and D. Gupta, Surf. Sci., 31 (1972), 566-585.

111. S. Vaidya, T. T. Sheng and A. K. Sinha, Appl. Phys. Lett., 36 (6) (1980), 464-466.

112. J. R. Lloyd, G. S. Hopper and W. B. Rousch, 20th Annual Reliability Physics Symposium, San Diego, California, IEEE, New York (1982), 47-49.

113. J. E. Baker, R. J. Blattner, S. Nadel and C. A. Evans, Thin Solid Films, 69 (1980), 53-62.

BIOGRAPHICAL SKETCH

Susan Matts Goho was born 9 June 1954 in Middlesex, New Jersey. The author attended Middlesex High School and graduated in 1972. She received a B. A. degree from Gettysburg College in Gettysburg, Pennsylvania in May 1976 with a major in both physics and mathematics. During the summer of 1974 and again, in the summer of 1975, she examined the lasing properties of CdS when pumped with a CO_2 laser pulse as a Summer Research Associate with Bell Laboratories in Holmdel, New Jersey. The author was then employed by AMP Incorporated in Harrisburg, Pennsylvania from December 1976 through August 1978. As a Jr. Research Engineer, she developed a computer model to describe the softening behavior of brass, bronze and nickel-silver alloys. She entered the Department of Materials Science and Engineering at the University of Florida as a graduate student in September 1978 and has pursued the degree of Doctor of Philosophy since that date.

The author has been a member of the American Physical Society since 1977 and a member of the American Vacuum Society since 1979.

I certify that I have read this study and that in my opinion it conforms to acceptable standards of scholarly presentation and is fully adequate, in scope and quality, as a dissertation for the degree of Doctor of Philosophy.

R. E. Hummel

Rolf E. Hummel, Chairman
Professor of Materials Science
and Engineering

I certify that I have read this study and that in my opinion it conforms to acceptable standards of scholarly presentation and is fully adequate, in scope and quality, as a dissertation for the degree of Doctor of Philosophy.

Paul H Holloway

Paul H. Holloway
Professor of Materials Science
and Engineering

I certify that I have read this study and that in my opinion it conforms to acceptable standards of scholarly presentation and is fully adequate, in scope and quality, as a dissertation for the degree of Doctor of Philosophy.

Robert T. DeHoff

Robert T. DeHoff
Professor of Materials Science
and Engineering

I certify that I have read this study and that in my opinion it conforms to acceptable standards of scholarly presentation and is fully adequate, in scope and quality, as a dissertation for the degree of Doctor of Philosophy.

Stanley R. Bates

Stanley R. Bates
Associate Engineer of Materials
Science and Engineering

I certify that I have read this study and that in my opinion it conforms to acceptable standards of scholarly presentation and is fully adequate, in scope and quality, as a dissertation for the degree of Doctor of Philosophy.

Gar B. Hoflund

Gar B. Hoflund
Associate Professor of Chemical
Engineering

This dissertation was submitted to the Graduate Faculty of the College of Engineering and to the Graduate School, and was accepted as partial fulfillment of the requirements for the degree of Doctor of Philosophy.

December, 1983

Hubert A. Bevis

Dean, College of Engineering

Dean for Graduate Studies and Research